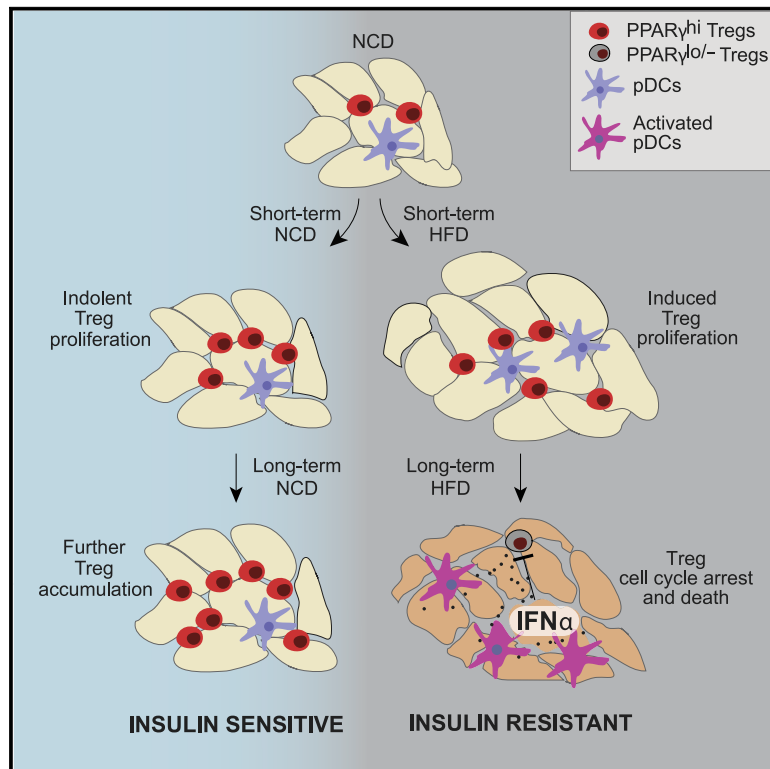


Cell Metabolism

Interferon- α -producing plasmacytoid dendritic cells drive the loss of adipose tissue regulatory T cells during obesity

Graphical abstract



Authors

Chaoran Li, Gang Wang,
Pulavendran Sivasami,
Ricardo N. Ramirez, Yanbo Zhang,
Christophe Benoist, Diane Mathis

Correspondence

chaoran.li@emory.edu (C.L.),
dm@hms.harvard.edu (D.M.)

In brief

Obesity-induced loss of insulin-sensitizing VAT-Tregs hinders the promise of Treg-based therapy for metabolic disorders. Li et al. demonstrate that VAT-Tregs decrease in obese mice in response to elevated levels of IFN- α made by local pDCs, which can be targeted to restore VAT-Tregs and insulin sensitivity.

Highlights

- Long-term, but not short-term, HFD feeding induces the loss of VAT-Tregs
- Obesity reduces VAT-Treg *Pparg* transcripts while inducing IFN-response transcripts
- Obesity-induced IFN- α , made by local pDCs, is directly toxic to VAT-Tregs
- Blocking the pDC-IFN α axis restores VAT-Tregs and insulin sensitivity



Article

Interferon- α -producing plasmacytoid dendritic cells drive the loss of adipose tissue regulatory T cells during obesity

Chaoran Li,^{1,2,3,*} Gang Wang,^{1,2} Pulavendran Sivasami,³ Ricardo N. Ramirez,^{1,2} Yanbo Zhang,^{1,2,4} Christophe Benoist,^{1,2} and Diane Mathis^{1,2,5,*}

¹Department of Immunology, Harvard Medical School, Boston, MA, USA

²Evergrande Center for Immunologic Diseases, Harvard Medical School and Brigham and Women's Hospital, Boston, MA 02115, USA

³Department of Microbiology and Immunology, Emory University School of Medicine, Atlanta, GA 30322, USA

⁴Present address: Cygnal Therapeutics, Cambridge, MA 02139, USA

⁵Lead contact

*Correspondence: chaoran.li@emory.edu (C.L.), dm@hms.harvard.edu (D.M.)

<https://doi.org/10.1016/j.cmet.2021.06.007>

SUMMARY

The visceral adipose tissue (VAT) of lean mice hosts a unique population of regulatory T cells (Tregs) that have a distinct transcriptome and T cell receptor (TCR) repertoire and regulate local and systemic inflammation and metabolism. Perplexingly, this population disappears in obese mice, limiting the promise of Treg-based therapies for metabolic disorders. We exploited the power of a VAT-Treg TCR-transgenic mouse model to follow the dynamics of, and phenotypic changes in, the VAT-Treg population throughout the development of diet-induced obesity. Our results show that VAT-Tregs are lost under obesogenic conditions due to down-regulation of their defining transcription factor, PPAR γ , coupled with their strikingly enhanced responses to pro-inflammatory cytokines. In particular, the VAT from obese mice (and reportedly humans) was strongly enriched in plasmacytoid dendritic cells that actively express interferon-alpha. These cells were directly toxic to PPAR γ ⁺ VAT-Tregs. Blocking this pathway in obese mice by multiple approaches substantially restored the VAT-Treg population and enhanced insulin sensitivity.

INTRODUCTION

Individuals with obesity are prone to a cluster of disorders termed the “metabolic syndrome,” which includes type 2 diabetes (T2D), heart disease, and stroke. Chronic, low-grade inflammation of the adipose tissue, and eventually systemically, is a major driver of obesity-associated metabolic disorders (Hotamisligil, 2017; Lee et al., 2018). The visceral adipose tissue (VAT) of lean individuals is enriched in classes of immunocytes that keep this inflammation in check in order to maintain tissue homeostasis, notably anti-inflammatory macrophages (MFs), type 2 innate lymphoid cells (ILC2s), and regulatory T cells (Tregs). In states of obesity, however, this anti-inflammatory condition is perturbed, resulting in the accumulation of several types of pro-inflammatory immunocytes; for example, pro-inflammatory MFs, natural killer (NK) cells, CD8⁺ T cells and CD4⁺ T helper (Th) type 1 cells, resulting in elevated levels of pro-inflammatory cytokines, such as tumor necrosis factor (TNF)- α , interleukin (IL)-6, interferons (IFNs), and IL-1 β . Such a drastic shift in the inflammatory tenor begs the question of how obesity renders the anti-inflammatory arm of the immune system incapable of properly controlling inflammation and maintaining adipose-tissue homeostasis.

Foxp3⁺CD4⁺ Tregs are critical guardians of the anti-inflammatory state of the VAT in lean individuals (Panduro et al., 2016).

Compared with their lymphoid-tissue counterparts, VAT-Tregs, in particular those in the epididymal fat depot, display a distinct, clonally expanded, repertoire of T cell receptors (TCRs), indicative of specific antigen recognition (Feuerer et al., 2009; Kolodin et al., 2015). In addition, VAT-Tregs have a unique transcriptome, largely driven by the nuclear receptor family member, PPAR γ (Cipolletta et al., 2012), the “master-regulator” of adipocyte differentiation. The accumulation of VAT-Tregs depends critically on the expression of Foxp3, specific TCRs and PPAR γ (Li et al., 2018), as well as on interactions with subtypes of VAT mesenchymal stromal cells that produce the cytokine, IL-33 (Vasanthakumar et al., 2015; Kolodin et al., 2015; Spallanzani et al., 2019). VAT-Tregs are highly represented in 20- to 30-week-old lean mice, reaching as high as 50%–80% of the CD4⁺ T cell compartment, but are reduced to 10%–20% levels with severe obesity (Feuerer et al., 2009; Deiuliis et al., 2011). In addition, the Tregs that persist in the VAT of obese mice show reduced expression of VAT-Treg signature genes such as *Klrg1*, *Ccr2*, *Il1r1*, and *Il10* (Cipolletta et al., 2015). Depletion of VAT-Tregs in lean mice leads to increased expression of inflammatory genes and reduced insulin sensitivity, while augmentation of VAT-Tregs during the course of obesity (e.g., by co-administration of a PPAR γ agonist) can improve metabolic indices (Feuerer et al., 2009; Eller et al., 2011; Cipolletta et al., 2012). These



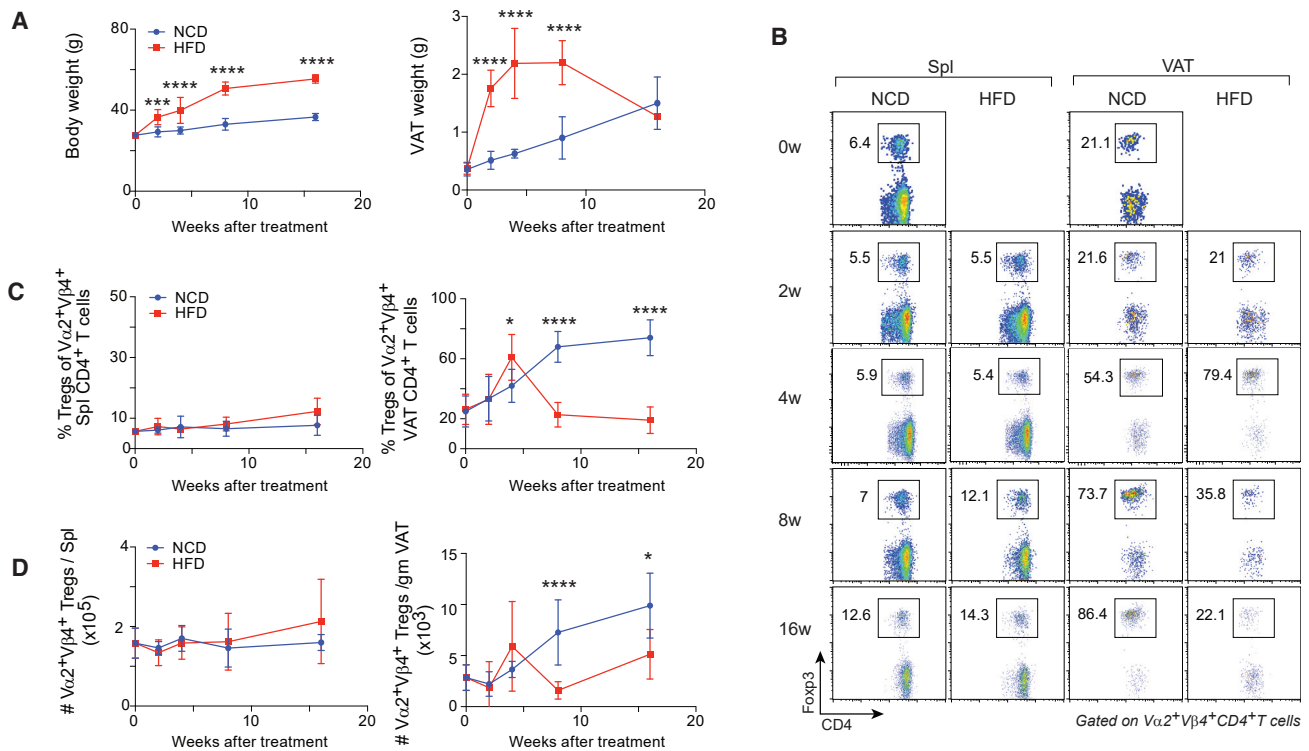


Figure 1. Evolution of the VAT-Treg compartment of vTreg53 TCR-tg mice with HFD feeding

(A–D) 12-week-old male vTreg53 TCR-tg *Foxp3-GFP* mice were fed either an NCD or an HFD for the indicated durations ($n \geq 4$ from 3 or 4 independent experiments, biological replicates). Mean \pm SD.

(A) Summary plots of body (left) and VAT (right) weights.

(B) Representative flow cytometry plots ($n \geq 4$, biological replicates) of Tregs. w, weeks of treatment. Numbers in the plots indicate the frequencies of Foxp3⁺ Tregs among $V\alpha 2^+ V\beta 4^+ CD4^+$ T cells.

(C) Frequencies of Tregs among clonotype⁺ CD4⁺ T cells from spleen (left) or VAT (right).

(D) Numbers of clonotype⁺ Tregs from spleen (left) or VAT (right).

* $p < 0.05$, *** $p < 0.001$, **** $p < 0.0001$ by 2-way ANOVA (A, C, and D).

findings argue that the dysregulation of VAT-Tregs is one of the major promoters of obesity-associated inflammation and metabolic abnormalities.

Some progress has been made in identifying the mechanisms underlying the loss of VAT-Tregs with obesity (Li et al., 2020). However, most of the relevant studies focused on animal models of severe obesity, such as mice fed a long-term (>8–20 weeks) high-fat diet (HFD) or genetically obese mice. Thus, only a late snapshot was taken, and we still lack a detailed view of the dynamics of the VAT-Treg population and its evolution during the onset, progression, and late phases of obesity. In addition, such analyses are often complicated by the heterogeneity of Tregs present in the VAT, potentially consisting of both true antigen-specific VAT-Tregs that reside in the tissue long-term and polyclonal cells that are circulating through or have been installed temporarily. Consequently, there is often great inter-individual variability in the kinetics and severity of the downstream consequences of obesity. To circumvent these issues, we took advantage of the recently generated vTreg53 TCR-transgenic(tg) mouse line, which hosts a large population of bona fide VAT-Tregs at a young age (10- to 12-weeks-old) and shows more homogeneous inflammatory and metabolic indices (Li et al., 2018). We traced the dynamics of and transcriptional changes in the

VAT-Treg population of vTreg53 TCR-tg mice during the development of HFD-induced obesity. VAT-Tregs responded in two distinct stages: an early expansion phase characterized by increased activation, proliferation, and maturation and then a sharp contraction phase accompanied by a loss of the distinct VAT-Treg transcriptome. The late response was associated with reduced *Pparg* expression and increased signaling by inflammatory cytokines, notably by IFN- α produced by local plasmacytoid dendritic cells (pDCs). These findings highlight new therapeutic options for mitigating the effects of obesity.

RESULTS

The response of VAT-Tregs to HFD feeding occurs in two distinct phases

To examine the behavior of VAT-Tregs during the onset, progression, and late phases of obesity, we fed 12-week-old vTreg53 TCR-tg mice either a normal-chow diet (NCD) or an HFD for 2, 4, 8, or 16 weeks; we then examined the frequencies and numbers of clonotype⁺ Tregs from the spleen and VAT. As expected, mice switched to an HFD gained significantly more body weight compared with those maintained on an NCD (Figure 1A). The VAT weight had increased dramatically by as early

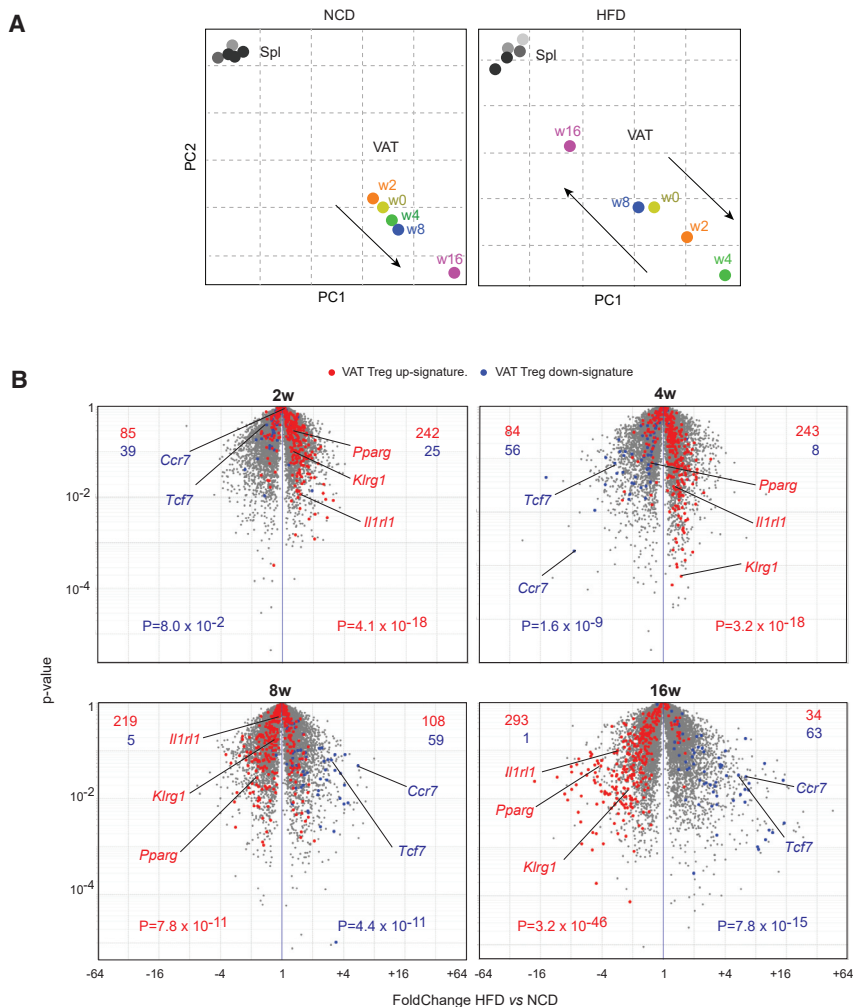


Figure 2. Global transcriptional changes induced in VAT-Tregs by an HFD challenge

(A and B) Mice were treated as in Figure 1, and clonotype⁺ Tregs were sorted for RNA-seq analysis (n = 2 or 3). Each dot represents the mean of 2–3 biological replicates.

(A) Principal component analyses of transcriptomes of clonotype⁺ splenic or VAT-Tregs at various time points. PCA was done using all samples (Spl and VAT, NCD and HFD) and then separated into two plots for easier visualization. spl, spleen; w, weeks; PC, principal component.

(B) Volcano plots comparing transcriptomes of clonotype⁺ VAT-Tregs from mice fed an HFD versus NCD for the indicated durations. The VAT-Treg up- and down-signatures have been reported (Cipolletta et al., 2015). Representative VAT-Treg up- and down-signature genes were highlighted. Figures at the top indicate the number of genes up- (red) or down- (blue) regulated by one or the other population.

p value is determined by a chi-square test (B).

as 2 weeks of HFD feeding but contracted at later times (8–16 weeks) (Figure 1A), potentially reflecting increased fibrosis and adipocyte death (Rosen and Spiegelman, 2014). Consistent with previous reports (Feuerer et al., 2009; Cipolletta et al., 2015), while the frequency and number of clonotype⁺ Tregs in the spleen of mice fed an NCD remained largely unaltered, those in the VAT increased substantially as the mice aged, starting at around 20% of the CD4⁺ T cell population and reaching as high as 70%–80% by 8–16 weeks (Figures 1B–1D). In contrast, in mice fed an HFD, the VAT-Treg population increased during the early phase (2–4 weeks), attaining more than 60% of the CD4⁺ T cell compartment, but then declined to only about 20% at 8–16 weeks (Figures 1B–1D).

We next compared how the transcriptomes of Tregs evolved over the course of HFD versus NCD feeding by conducting population-level RNA-seq on double-sorted clonotype⁺ spleen and VAT-Tregs. Principal component analysis (PCA) was performed on the four samples (spleen and VAT under NCD and HFD), which were then separated into two plots (NCD and HFD) for easier visualization (Figure 2A). The Treg transcriptomes segregated primarily by their tissue of origin. The transcriptional profile of spleen Tregs remained quite constant throughout the time

course of both NCD and HFD feeding. In mice fed an NCD, the VAT-Treg transcriptome gradually evolved as the mice aged, becoming more and more distinct from the transcriptional profiles of their splenic counterparts (Figure 2A, left). On the HFD, the transcriptome of VAT-Tregs diverged from the transcriptional profiles of splenic Tregs at 2 and 4 weeks, but then gradually lost the distinguishing features and became more like the profiles of splenic Tregs at 8 and 16 weeks (Figure 2A, right). In agreement with the PCA, our previously established VAT-Treg up- and down-signatures (Cipolletta et al., 2015) were more

prominent in clonotype⁺ VAT-Tregs of mice fed an HFD than an NCD at the early time points, suggesting that either short-term HFD accelerated the maturation of VAT-Tregs or that there was a higher fraction of bona fide VAT Tregs (as opposed to “interlopers”). In contrast, with prolonged HFD feeding, VAT-Tregs showed reduced expression of VAT-Treg up-signature genes, indicative of a loss of the distinct VAT-Treg features (Figure 2B).

Collectively, these results indicate that with HFD feeding the size of the VAT depot as well as the representation of VAT-Tregs evolved in two distinct stages: an early expansion phase and a late contraction phase. The VAT-Treg transcriptome changed in parallel.

The onset and progression of obesity are associated with alterations in the proliferation and death of VAT-Tregs

Gene set enrichment analysis (GSEA) of the RNA-seq data revealed which pathways were modulated during the onset and progression of obesity. VAT-Tregs from mice fed an HFD for 2 weeks showed increased expression of genes related to cell activation and proliferation (e.g., Myc targets, E2F targets and the p53 pathway) (Figure 3A), in agreement with the accelerated

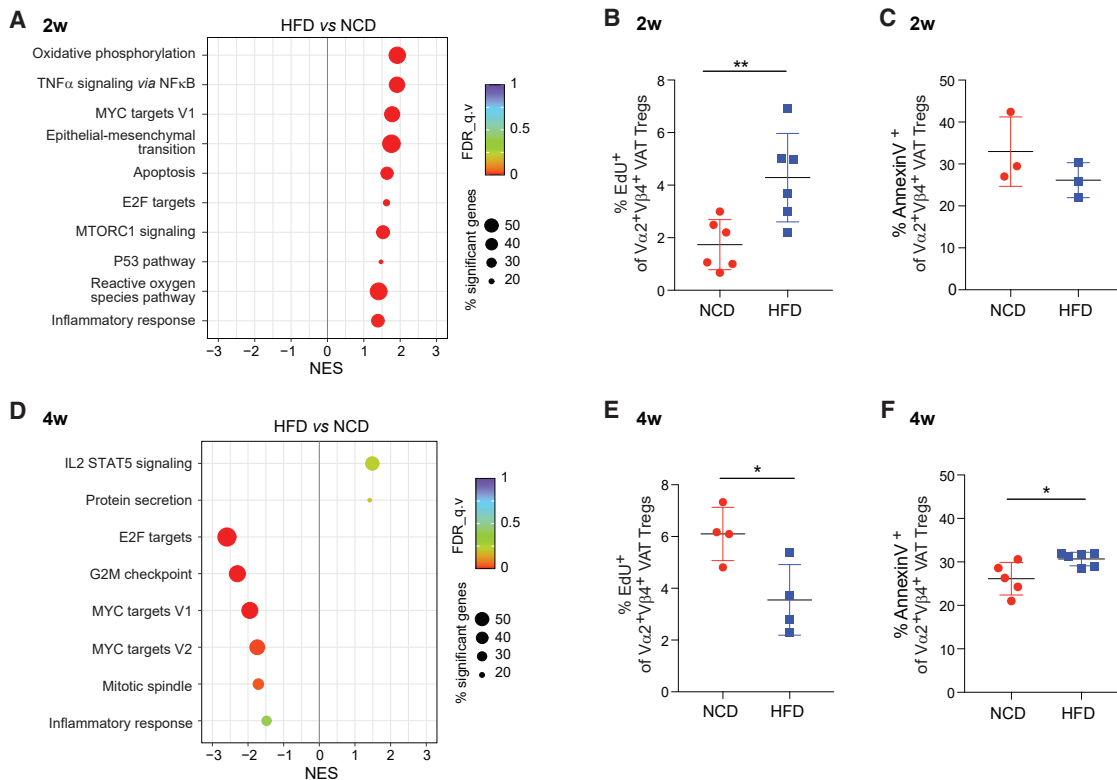


Figure 3. Early changes in VAT-Treg dynamics upon HFD feeding

(A) GSEA showing the KEGG pathways most enriched or impoverished in clonotype⁺ VAT-Tregs at 2 weeks of HFD, in comparison with NCD, feeding ($p < 0.05$). NES, normalized enrichment score; FDR, false discovery rate.

(B) Proliferation of clonotype⁺ VAT-Tregs at 2 weeks of NCD or HFD feeding. Mice were pulsed for 5 h with EdU, at which time tissues were flow-cytometrically analyzed for incorporation ($n = 6$, biological replicates).

(C) Flow-cytometrically determined frequencies of annexin V⁺ clonotype⁺ Tregs isolated from mice fed NCD or HFD for 2 weeks ($n = 3$, biological replicates).

(D–F) Same as A–C except mice were fed NCD versus HFD for 4 weeks ($n \geq 4$, biological replicates).

Summary plots show data pooled from 2 or 3 independent experiments. Mean \pm SD.

* $p < 0.05$, ** $p < 0.01$ by unpaired Student's *t* test (B, C, E, and F).

accumulation of VAT-Tregs during the early phases of obesity (Figures 1B and 1C). Indeed, a 5-h *in vivo* pulse of the nucleoside analog, 5-ethynyl-20-deoxyuridine (EdU), demonstrated a higher proportion of dividing clonotype⁺ VAT-Tregs in vTreg53 TCR-tg mice fed an HFD compared with an NCD for 2 weeks (Figure 3B). Although GSEA also uncovered an increase in transcripts indicative of apoptosis at this time point, we could not confirm this association by annexin V staining of VAT-Tregs freshly isolated *ex vivo* (Figure 3C). These results suggest that the accelerated accumulation of VAT-Tregs during the onset of obesity is mainly driven by increased proliferation, rather than by reduced turnover.

In striking contrast, VAT-Tregs from mice fed an HFD for 4 weeks were relatively low in transcripts associated with proliferation and the cell cycle (e.g., E2F targets, G2M checkpoint, Myc targets, and mitotic spindle) (Figure 3D). And flow-cytometric analysis confirmed that the proportion of dividing Tregs was lower, while that of annexin V⁺ cells was greater, in the VAT of mice fed 4 weeks of HFD (compared with NCD) (Figures 3E and 3F). Therefore, although still at their peak of accumulation at 4 weeks of HFD feeding (Figures 1B–1D), VAT-Tregs already

exhibited clear signs of cell-cycle arrest and greater cell death. Perhaps not surprisingly, by 8 weeks after the introduction of HFD, the residual VAT-Treg survivors no longer showed any differences in cell proliferation or apoptosis (Figures S1A and S1B).

Prolonged HFD feeding is associated with loss of the distinct VAT-Treg transcriptome and with increased responses to pro-inflammatory cytokines

At 8 and 16 weeks after the introduction of HFD feeding, GSEA revealed strong inductions of transcripts indicative of responses to the pro-inflammatory cytokines IFN- α , TNF- α , and IFN- γ , while known hallmarks of VAT-Tregs—including the cholesterol homeostasis, peroxisome, and fatty-acid metabolism pathways—were significantly lower (Figures 4A and 4B). k-means clustering of the transcripts differentially expressed by VAT-Tregs over the course of HFD versus NCD feeding ($p < 0.05$; FDR < 0.05 ; $r^2 > 0.65$) yielded similar findings, but with more detailed kinetics (Figure 4C). Cluster 1, enriched in transcripts encoding elements of the cholesterol homeostasis pathway (*Hmgcr*, *Hmgcs1*, *Ldlr*, etc.), was maintained at high levels under an NCD but was gradually lost with prolonged HFD feeding.

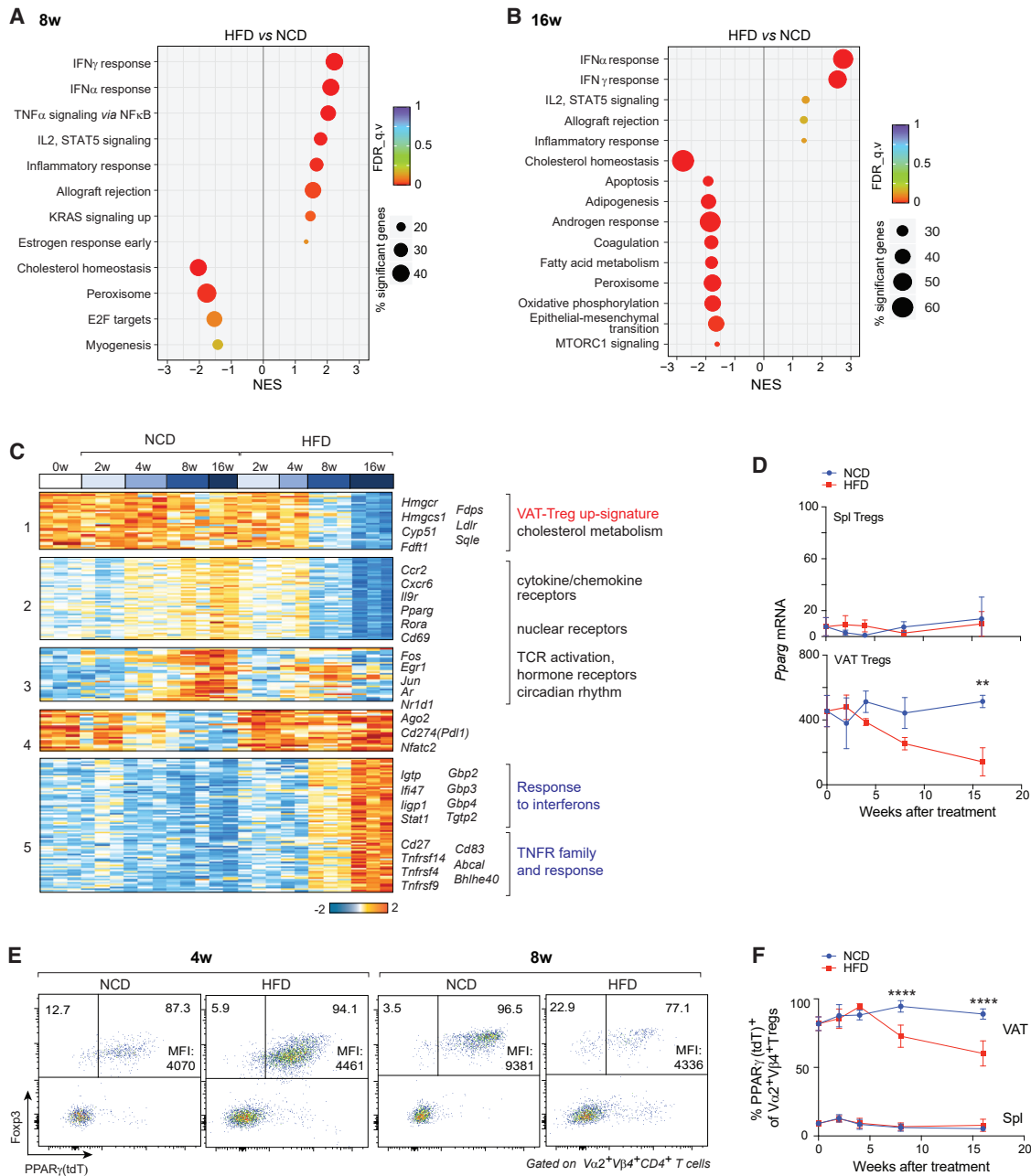


Figure 4. The late response of VAT Tregs to an HFD: PPAR γ downregulation and up-regulation of pro-inflammatory cytokine signaling (A and B) GSEA showing top KEGG pathways enriched or impoverished in clonotype⁺ VAT-Tregs at 8 (A) or 16 (B) weeks of HFD, compared with NCD, feeding ($p < 0.05$). (C) K-means clustering of transcripts expressed in clonotype⁺ VAT-Tregs differentially under NCD versus HFD conditions ($p < 0.05$, FDR < 0.05 , $r^2 \geq 0.65$). (D) RNA-seq quantification of *Pparg* transcript levels under the two feeding conditions ($n = 2$ or 3, biological replicates). (E) Representative flow-cytometric plots ($n \geq 3$, biological replicates) showing frequencies of PPAR γ (tdT)⁺ among clonotype⁺ VAT-Tregs. Numbers in the plots indicate the frequencies of PPAR γ (tdT)⁻ or PPAR γ (tdT)⁺ cells among clonotype⁺ Tregs. MFIs of PPAR γ (tdT) of only the PPAR γ (tdT)⁺ Tregs are indicated. (F) Summary plot showing frequencies of PPAR γ (tdT)⁺ cells among clonotype⁺ Tregs at various times after introduction of NCD or HFD ($n \geq 3$, biological replicates).

Summary plots show data pooled from two to three independent experiments. Mean \pm SD.

** $p < 0.01$, **** $p < 0.0001$ by two-way ANOVA (D and F).

Clusters 2 and 3—which included a number of VAT-Treg up-signature transcripts encoding cytokine or chemokine receptors (*Ccr2*, *Cxcr6*, and *Il9r*), nuclear receptors (*Pparg* and *Rora*), pro-

teins associated with TCR activation (*Cd69*, *Fos*, *Egr1*, and *Jun*), or circadian rhythm components (*Nr1d1*)—were increased under NCD feeding and with short durations of HFD feeding but

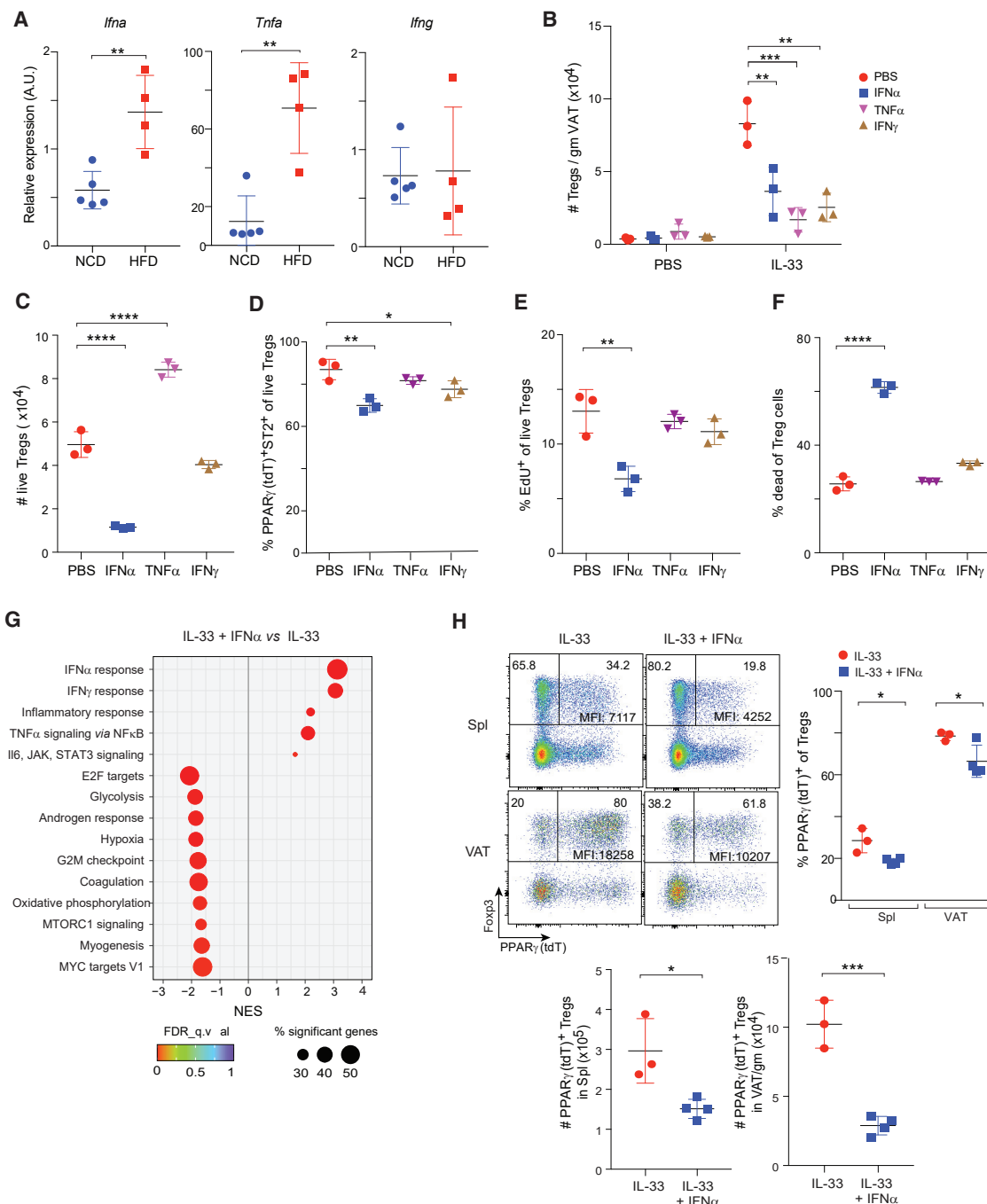


Figure 5. Roles of IFN- α , TNF- α , and IFN- γ in the loss of VAT-Tregs with HFD feeding

(A) Expression of the indicated cytokine genes in whole VAT tissue from vTreg53 TCR-tg mice fed 8 weeks on NCD or HFD as determined by RT-qPCR. ($n \geq 4$, biological replicates).

(B) Number of VAT-Tregs from 12-week-old B6 mice injected with various cytokines twice in a week ($n = 3$, biological replicates). PBS, phosphate-buffered saline.

(C–F) VAT-Tregs were treated with indicated cytokines *in vitro* for 4 days ($n = 3$, biological replicates).

(C) Numbers of live VAT-Tregs.

(D) Frequencies of PPAR γ (tdT) $^+$ ST2 $^+$ cells among live Tregs.

(E) Frequencies of live Tregs that had incorporated EdU in the last 2 h of culture.

(F) Frequencies of dead cells among Tregs.

(G) Transcriptome analysis of VAT-Treg cells treated *in vitro* for 3 days ($n = 2$ or 3, biological replicates). GSEA showing top KEGG pathways enriched or depleted in VAT-Treg cells treated with IL-33 + IFN- α compared with IL-33 alone.

(legend continued on next page)

declined with long-term exposure to an HFD. Cluster 4 transcripts, including *Ago2*, *Cd274*, and *Nfatc2*, were maintained at high levels throughout HFD feeding and with short-term NCD feeding but were reduced with prolonged NCD feeding. Cluster 5—consisting mainly of transcripts associated with the response to IFNs or TNF- α and those encoding TNF family members—was induced under long-term HFD feeding.

PPAR γ is a primary driver of VAT-Treg accumulation and phenotype (Cipolletta et al., 2012). While, as expected, VAT-Treg *Pparg* transcripts were maintained at high levels in mice on an NCD, they decreased with longer durations of HFD feeding (Figure 4D). Reduced *Pparg* expression in VAT-Tregs of mice on HFD was confirmed by examination of PPAR γ -reporter mice, which showed both fewer PPAR γ (tdT)⁺ cells and a lower mean fluorescence intensity (MFI) in those cells that were positive (Figures 4E and 4F).

In brief, then, the major transcriptomic hallmarks of long-term HFD feeding were loss of the diagnostic VAT-Treg signature and responses to inflammatory cytokines. These changes did not occur in splenic Tregs from the same mice.

IFN- α directly inhibits the proliferation and survival of PPAR γ ⁺ VAT-Tregs

The striking induction of transcripts indicative of responses to pro-inflammatory cytokines with prolonged HFD feeding prompted us to investigate whether these cytokines could inhibit the accumulation of VAT-Tregs. In agreement with previous reports (Ghosh et al., 2016; Hotamisligil et al., 1993), levels of *IFN- α* and *Tnfa* transcripts were significantly higher in VAT from mice fed 8 weeks on an HFD compared with those on an NCD; the abundance of *Ifng* transcripts was not higher at this time point (Figure 5A). Previous studies have shown that the accumulation of bona fide VAT-Tregs over time critically depends on the cytokine, IL-33 (Vasanthakumar et al., 2015; Kolodin et al., 2015); however, the amount of IL-33 in VAT is not reduced, but rather increased, under long-term HFD feeding (Spallanzani et al., 2019). Therefore, we hypothesized that pro-inflammatory cytokines might be able to antagonize IL-33-driven accumulation of VAT-Tregs. We injected two doses of IL-33 (3 days apart) into 8-week-old B6 mice and examined Treg compartments 7 days after the first injection. There was an impressive expansion of the Treg population in VAT (Figure 5B), and a much weaker one in spleen (Figure S2A). Injection of IFN- α , TNF- α , or IFN- γ along with IL-33 inhibited IL-33-induced expansion of the VAT-Treg population (Figure 5B). We did not observe noticeable effects of these cytokines on VAT-Tregs in the absence of IL-33, likely due to the slow turnover of VAT-Tregs (Kolodin et al., 2015) and the short duration of treatment.

The effect of these pro-inflammatory cytokines could be Treg-intrinsic or could reflect indirect influences on other cell types important for VAT-Treg accumulation, such as ILC2s. Indeed, and in agreement with results from previous studies

(Duerr et al., 2016; Moro et al., 2016; Oldenhove et al., 2018; Molofsky et al., 2015), the numbers of ILC2s were reduced by injection of IFN- α , TNF- α , or IFN- γ together with IL-33, in comparison with administration of IL-33 alone (Figures S2B and S2C). To determine whether any of the pro-inflammatory cytokines could directly antagonize IL-33-driven expansion of bona fide VAT-Tregs, we sorted PPAR γ (tdT)⁺ VAT-Tregs expanded *in vivo* with IL-33, and cultured them *in vitro* with IL-33 plus IFN- α , TNF- α , or IFN- γ . By four days of culture, there were much fewer surviving Tregs with the addition of IFN- α , but not with the other two cytokines (Figure 5C), and the survivors included a lower proportion of PPAR γ (tdT)⁺ST2⁺ cells (Figure 5D).

Mechanistically, examination of EdU incorporation and uptake of live/dead violet dead cell stain revealed that IFN- α suppressed both the proliferation and survival of VAT-Tregs, while TNF- α and IFN- γ did not (Figures 5E and 5F). Consistently, GSEA of RNA-seq data on VAT-Tregs treated with IL-33 + IFN- α versus IL-33 alone showed enrichment of the IFN and inflammatory responses under the former condition, and depletion of pathways associated with cell activation and proliferation (E2F targets, glycolysis, G2M checkpoint, oxidative phosphorylation) (Figure 5G). We also generated a “16-week-HFD signature” of transcripts that were up- or downregulated more than 2-fold in VAT Tregs from mice fed 16 weeks on HFD versus NCD (Table S1). Overlay of this signature on a volcano plot comparing gene expression by IFN- α + IL-33- versus IL-33-treated VAT Tregs revealed an enrichment of the 16-week-HFD-upregulated gene set and an impoverishment of the 16-week-HFD-downregulated gene set in the former group (Figure S2D). Therefore, many of the transcripts changed by long-term HFD feeding were also modulated by IFN- α . In addition, expression of *Icos*, which has been shown to be important for Treg proliferation, was not changed by IFN- α treatment in VAT-Tregs (Figure S2E).

We next investigated whether the impact of IFN- α was more pronounced in particular subtypes of Tregs, notably those expressing PPAR γ . Injection of IFN- α alone into 8-week-old *Pparg*-*tdT* *Foxp3*-*GFP* mice did not alter the frequencies of PPAR γ ⁺ Tregs in the spleen and VAT, although it did reduce the level of PPAR γ in these cells (Figures S2F and S2G). We have shown previously that IL-33 injection leads to a significant increase in the proportion of PPAR γ ⁺ Tregs (Li et al., 2018). Interestingly, compared with injection of IL-33 alone, co-injection of IFN- α and IL-33 into 8-week-old *Pparg*-*tdT* *Foxp3*-*GFP* mice led to a significant reduction in the proportions and numbers of PPAR γ ⁺ Tregs, as well as PPAR γ (tdT) expression levels, in both spleen and VAT (Figure 5H).

These results indicate that, while multiple pro-inflammatory cytokines were toxic to VAT-Tregs, only IFN- α had a direct effect. This cytokine inhibited VAT-Treg accumulation through effects on both proliferation and survival.

(H) 8-week-old PPAR γ -*Tdt* *Foxp3*-*GFP* mice were injected with two doses of IL-33 alone or IL-33 + IFN- α in a week ($n \geq 3$, biological replicates). Top left panels: representative flow-cytometric dot plots of PPAR γ (tdT)⁺ Tregs. Numbers in the plots indicate the frequencies of PPAR γ (tdT)⁻ or PPAR γ (tdT)⁺ cells among Tregs. MFI of PPAR γ (tdT) for only the PPAR γ (tdT)⁺ Tregs is shown. Top right panels: frequencies of PPAR γ (Tdt)⁺ Tregs from spleen and VAT. Bottom panels: numbers of PPAR γ (tdT)⁺ Tregs.

Summary plots show data pooled from two to three independent experiments. Mean \pm SD.

* $p < 0.05$, ** $p < 0.01$, *** $p < 0.001$, **** $p < 0.0001$ by unpaired Student's *t* test (A and H bottom), one-way ANOVA (C–F), or two-way ANOVA (B and H, top).

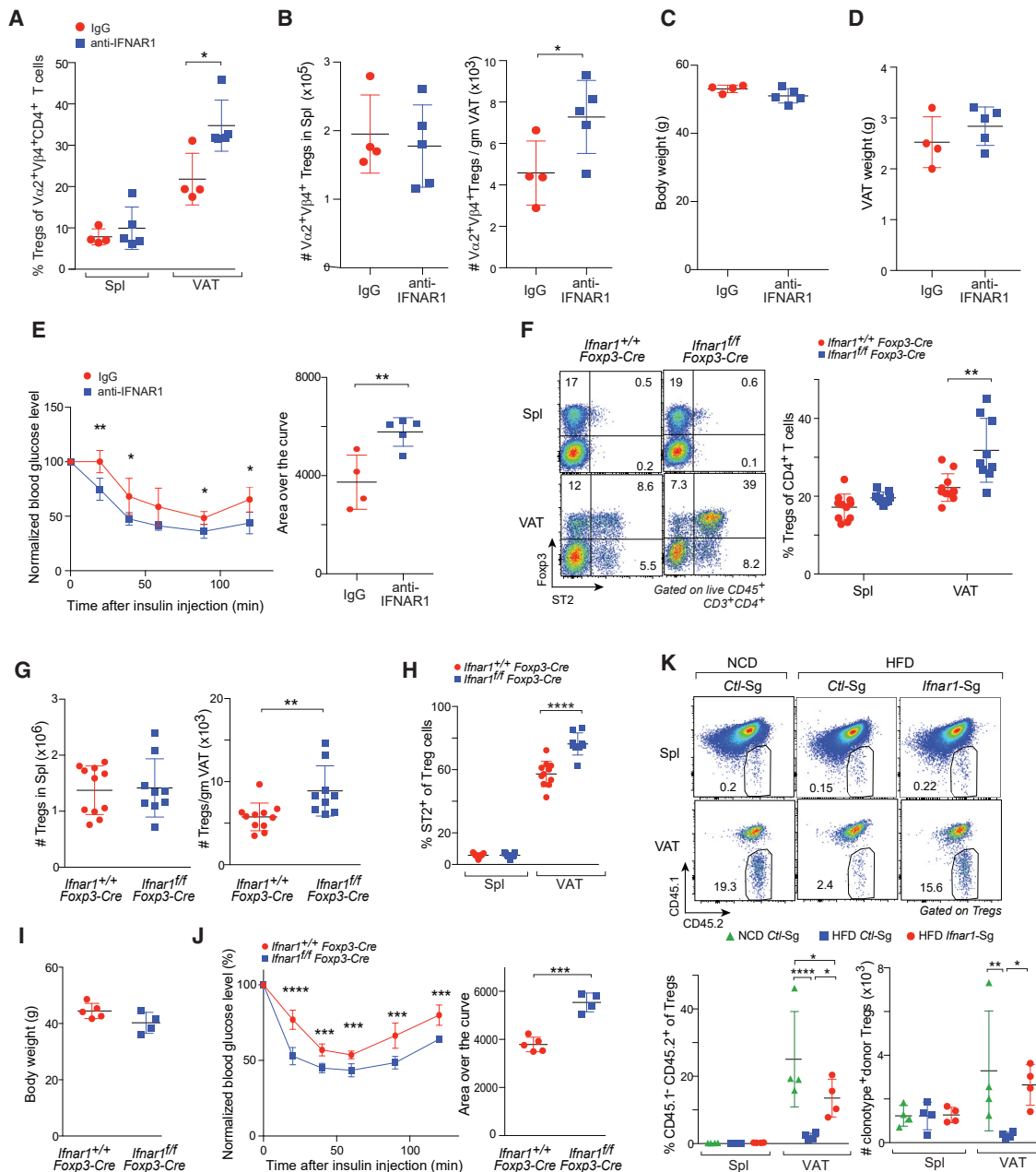


Figure 6. Systemic blockade or Treg-specific knockout of IFNAR1 substantially rescued the VAT-Treg compartment and improved insulin sensitivity in conditions of HFD feeding

(A–E) 12-week-old vTreg53 TCR-tg mice were fed on HFD and injected with an anti-IFNAR1 or isotype-control Ab (IgG) i.p. twice a week for 8 weeks (n ≥ 4, biological replicates).

(A) Frequencies of clonotype⁺ Tregs. Spl, spleen.

(B) Numbers of clonotype⁺ splenic (left) or VAT- (right) Tregs.

(C) Body weight.

(D) VAT weight.

(E) Insulin tolerance test (ITT): normalized blood glucose levels over time (left); area over the curve (AOC) (right).

(F–J) 12-week-old *Ifnar1^{fl/fl}* or *Ifnar1^{+/+} Foxp3-cre* mice were fed on HFD for 8 weeks.

(F) Frequencies of Tregs (n ≥ 9, biological replicates). Left: representative flow-cytometric plots of ST2⁺ Tregs. Numbers in the plots indicate the frequencies of cells in each gate. Right: summary plot.

(G) Numbers of Tregs in the spleen (left) and VAT (right). (n ≥ 9, biological replicates).

(H) Frequencies of ST2⁺ cells in Tregs. (n ≥ 9, biological replicates).

(I) Body weight. (n ≥ 4, biological replicates).

(legend continued on next page)

Signaling via IFNAR1 on VAT-Tregs drives their loss with prolonged HFD feeding

Type-I IFNs (IFN- α and IFN- β) signal through a common heterodimeric receptor consisting of two subunits, IFNAR1 and IFNAR2 (Barrat et al., 2019). To determine whether heightened type-I IFN production was actually responsible for the reduction in VAT-Tregs under prolonged HFD feeding (and not just capable of causing it), we fed 12-week-old vTreg53 TCR-tg mice an HFD and injected them with either a blocking anti-IFNAR1 monoclonal antibody (mAb) or an IgG isotype-control mAb twice a week for 8 weeks. Blockade of IFNAR1 increased both the proportion and number of clonotype⁺ Tregs in VAT but not in the spleen (Figures 6A and 6B). In addition, the frequencies and numbers of CD11c^{hi} inflammatory macrophages in VAT were lower in mice treated with anti-IFNAR1 compared with those treated with IgG mAb (Figure S3A), likely as a result of higher VAT-Tregs in these mice. Remarkably, while body and VAT weights were comparable for the two groups (Figures 6C and 6D), insulin sensitivity was significantly improved by anti-IFNAR1 treatment (Figure 6E).

As many cell types express IFNAR1 and could potentially mediate the benefits observed after anti-IFNAR1 mAb treatment, we determined whether ablation of IFNAR1 on Tregs alone was sufficient to confer these effects. In addition, we wanted to extend our observations to a polyclonal setting. Thus, we generated 12-week-old *Ifnar1^{fl/fl}* and *Ifnar1^{+/+} Foxp3-cre* mice and fed them an HFD for 8 weeks. Consistent with the anti-IFNAR1 mAb treatment, the frequencies and numbers of VAT-Tregs as well as the fraction of ST2⁺ Tregs in VAT were significantly increased in *Ifnar1^{fl/fl} Foxp3-Cre* mice compared with *Ifnar1^{+/+} Foxp3-cre* littermates (Figures 6F–6H). Importantly, *Ifnar1^{fl/fl} Foxp3-Cre* mice had body weights that were similar to those of *Ifnar1^{+/+} Foxp3-Cre* littermates that had undergone the same treatment, but they were significantly more insulin sensitive (Figures 6I and 6J).

As a second approach to assessing the importance of IFNAR1 specifically on Tregs, we set up an adoptive-transfer system. vTreg53 TCR-tg mice were crossed with mice constitutively expressing CRISPR-associated protein 9 (Cas9) from the *Rosa26* locus. Tregs were purified from pooled spleen and lymph nodes of CD45.1⁺CD45.2⁺ TCR-tg⁺ Cas9^{KI/WT} *Foxp3-thy1.1^{KI/y}* mice and were transduced with retroviral constructs expressing a single guide RNA (sgRNA) targeting *Ifnar1* (*Ifnar1*-Sg) or a control non-targeting sgRNA (*Ctl*-Sg). The transduced cells (labeled by GFP) were transferred into 12-week-old CD45.1⁺CD45.2⁺ Cas9^{KI/WT} recipients, which were then fed either an NCD or an HFD for 8 weeks (see Figure S3B for the experimental scheme). As expected, transduction of *Ifnar1*-Sg resulted in efficient ablation of IFNAR1 on Tregs (Figure S3C). In agreement with our previous report (Li et al., 2018), *Ctl*-Sg-transduced Tg⁺ Tregs preferentially accumulated in VAT (versus spleen) after transfer into mice fed an NCD; and this build-up was strongly attenuated in recipient mice fed an HFD (Figure 6K). Remarkably, ablation of

IFNAR1 only on Tregs largely resurrected the accumulation of transferred Tg⁺ Tregs in VAT of mice fed an HFD (Figure 6K). (Note: in transfer systems like this one and the one below, too few Tregs accumulate in VAT to be able to impact metabolic indices.)

As an alternative strategy, we transduced Tregs from CD45.2⁺ TCR-tg⁺ Cas9^{KI/WT} mice with retroviral constructs expressing *Ifnar1* or *Ctl* SgRNAs (cells labeled with GFP or mRFP, respectively), mixed them at a 1:1 ratio, and transferred the mixture into recipient mice that were subsequently fed an HFD. After 8 weeks, while the fractions of *Ifnar1*-Sg-transduced and *Ctl*-Sg-transduced donor-derived Tregs were quite similar in the spleen, there were clearly more of the former in the VAT of recipient mice (Figure S3D).

These findings demonstrate that the suppression of VAT-Treg cell accumulation by long-term HFD feeding was largely due to a direct effect of increased type-I IFN levels, and that ablation of IFNAR1 specifically on Tregs was sufficient to attenuate their reduction upon HFD feeding and improve metabolic indices in obese mice. Considered together with the gain-of-function results depicted in Figure 5, these loss-of-function data constitute a strong argument for the primacy of these pro-inflammatory cytokines.

pDCs are enriched in VAT with long-term HFD feeding, produce substantial levels of IFN- α and suppresses VAT-Treg accumulation

pDCs are a unique population of immunocytes that secrete large amounts of IFN- α in response to viral infections or in certain autoimmune conditions (Liu, 2005). Thus, we wondered whether changes in this cell population might underlie the higher IFN- α expression in mice on an HFD. Indeed, the frequency and number of pDCs (identified by the markers PDCA-1 and Ly6c) were strongly elevated in VAT of mice fed an HFD for 8 weeks (Figure 7A). This increase was evident already 4 weeks after the introduction of HFD (Figure 7B), correlating well with the time point when the representation of VAT-Tregs and their expression of PPAR γ began to decline (Figures 1C and 4D).

To evaluate the impact of pDCs on VAT-Tregs under obesogenic conditions, we obtained *Bdca2-Dtr* mice, wherein injection of diphtheria toxin (DT) leads to highly specific depletion of pDCs (Swiecki et al., 2010). 10-week-old *Bdca2-Dtr⁺* or *Dtr⁻* littermates were fed an HFD for 4 weeks, after which they were continued on an HFD while being injected intraperitoneally (i.p.) with DT twice a week for another 4 weeks. DT was administered only for the latter 4 weeks of HFD feeding to avoid induction of neutralizing Abs upon chronic treatment and because pDCs started to accumulate only after 4 weeks of HFD feeding (Figure 7B). DT treatment of *Bdca2-Dtr⁺* mice indeed led to a specific depletion of pDCs (identified by markers including PDCA-1, Ly6c, Siglec-H, and B220) and a reduction in IFN- α transcript levels compared with those of *Dtr⁻* littermates (Figures 7C and

(J) Insulin tolerance test (ITT). Normalized blood glucose levels over time (left); area over the curve (AOC) (right). ($n \geq 4$, biological replicates).

(K) Effect of CRISPR-Cas9-mediated ablation of *Ifnar1* in vTreg53 TCR-tg Tregs on their enrichment in VAT following transfer into NCD- or HFD-fed mice ($n = 4$, biological replicates). Top: representative flow-cytometric dot-plot of donor-derived Tregs. Numbers in the plots indicate the frequencies of donor-derived cells among total Tregs. Bottom: frequencies and numbers of donor-derived Tregs.

Summary plots show data pooled from two to three independent experiments. Mean \pm SD.

* $p < 0.05$, ** $p < 0.01$, *** $p < 0.001$, **** $p < 0.0001$ by unpaired Student's t test (B, E right, G, J right) or two-way ANOVA (A, E left, F, H, J left, K bottom).

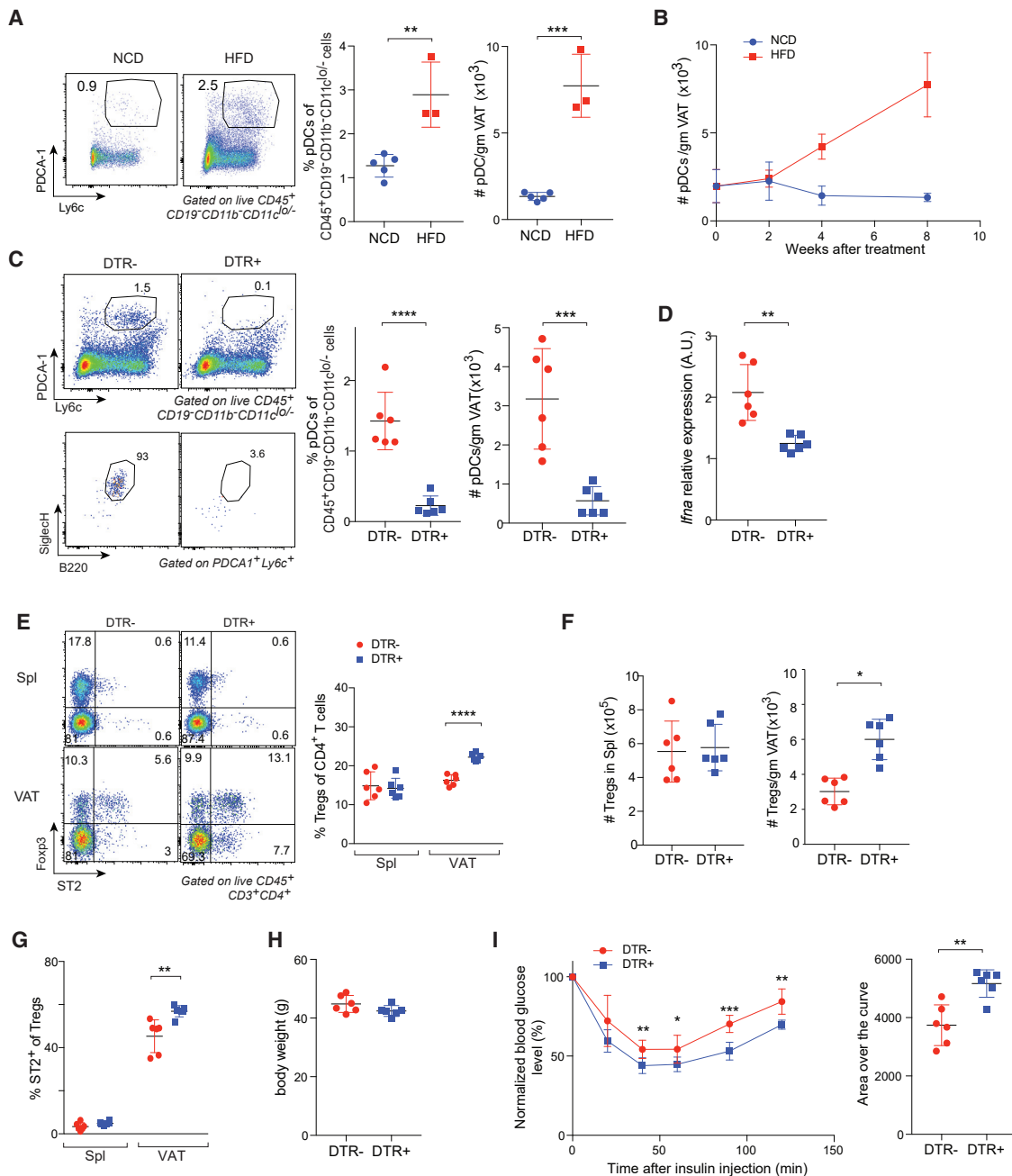


Figure 7. IFN- α -expressing pDCs increase in the VAT during prolonged HFD feeding and inhibit VAT-Treg accumulation

(A) Frequencies and numbers of pDCs from VAT of vTreg53 TCR-tg mice fed on NCD or HFD for 8 weeks ($n \geq 3$, biological replicates). Left: representative flow-cytometric dot plots of pDCs. Numbers in the plots indicate the frequencies of pDCs among CD45⁺ CD19⁻ CD11b⁻ CD11c^{Lo/-} cells. Center and right: summary data.

(B) Time course of pDC numbers from VAT of vTreg53 TCR-tg mice fed an NCD or HFD beginning at 12 weeks of age ($n \geq 3$, biological replicates).

(C) pDCs from VAT of HFD-fed, DT-treated *Bdca2-Dtr⁺* or *Dtr⁻* mice ($n = 6$, biological replicates) Left: representative flow-cytometric dot plots of pDCs. Numbers in the plots indicate the frequencies of PDCA-1⁺ Ly6c⁺ cells among CD45⁺ CD19⁻ CD11b⁻ CD11c^{Lo/-} cells (top left) or the frequencies of B220⁺ SiglecH⁺ cells among PDCA-1⁺ Ly6c⁺ cells (bottom left). Center and right: summary data showing frequencies and numbers of pDCs in VAT.

(D) qRT-PCR quantification of *IFN- α* transcript levels from whole VAT tissue of HFD-fed, DT-treated *Bdca2-Dtr⁺* or *Dtr⁻* mice ($n = 6$, biological replicates). a.u., arbitrary units.

(E) Frequencies of Tregs from spleen and VAT of HFD-fed, DT-treated *Bdca2-Dtr⁺* or *Dtr⁻* mice ($n = 6$, biological replicates). Left: representative flow-cytometric dot plots of ST2⁺ Tregs. Numbers in the plots indicate the frequencies of cells in each gate. Right: summary data.

(F) Numbers of Tregs from spleen (left) and VAT (right) of HFD-fed, DT-treated *Bdca2-Dtr⁺* or *Dtr⁻* mice ($n = 6$, biological replicates).

(G) Frequencies ST2⁺ cells in Spl or VAT Tregs ($n = 6$, biological replicates).

(legend continued on next page)

7D). There were significant increases in the frequencies and numbers of Tregs as well as in their ST2 expression levels on VAT—but not spleen—Tregs (Figures 7E–7G). DT-treated *Bdca2-Dtr⁺* mice had body weights similar to those of *Bdca2-Dtr⁻* littermates that received the same treatment, but they were more insulin sensitive (Figures 7H and 7I).

Because of its translational implications, and although it might not be as specific an approach under inflammatory conditions (Blasius et al., 2006), we also punctually ablated pDCs using a mAb. pDCs in vTreg53 TCR-tg mice were continuously depleted using anti-PDCA-1 and the VAT-Treg population was examined after 8 weeks of HFD feeding. As expected, depletion of VAT pDCs under these conditions resulted in a significant reduction in whole-tissue *IFN- α* transcript levels (Figure S4A). Strikingly, pDC depletion significantly increased the clonotype⁺ VAT-Treg population (Figure S4B), particularly those cells expressing PPAR γ (Figure S4C). Lastly, while the body and VAT weights were comparable between vTreg53 TCR-tg⁺ mice treated with α -PDCA1 and control-IgG (Figures S4D and S4E), pDC-depleted mice exhibited a clear improvement in insulin sensitivity (Figure S4F).

In short, these results—obtained from both a constitutive and a punctual depletion system—strongly argue that type-I IFN, largely produced by pDCs, was a major driver of the loss of VAT-Tregs and their PPAR γ expression during prolonged HFD feeding.

DISCUSSION

VAT-Tregs safeguard VAT homeostasis and, thereby, metabolic health. Hence, they have been thought to be a promising therapeutic target for treating obesity-associated metabolic disorders. Unfortunately, the use of Treg-based therapy in this context is hindered by the induction of an adipose-tissue microenvironment that is toxic to VAT-Tregs in individuals with obesity. The major goals of our study were to explore the dynamics of VAT-Tregs during the onset, progression, and late phases of obesity and to elucidate mechanisms underlying the eventual dysregulation of VAT-Tregs. Our data indicate that VAT-Tregs responded to obesity in two distinct stages. Short-term feeding on an HFD induced expansion of the gonadal VAT depot and accelerated the proliferation and potentially the maturation of VAT-Tregs. However, prolonged HFD feeding exceeded the expansion capacity of this adipose depot, resulting in regression of the VAT mass. This effect was associated with the accumulation and activation of pDCs that expressed high levels of *IFN- α* , which directly inhibited VAT-Treg accumulation, eventually resulting in a compartment lacking the typical VAT-Treg characteristics.

The impressive increase in VAT-Tregs shortly after the introduction of an HFD was somewhat unexpected and raises questions as to its causation and biological meaning. Our results argue that this increase was largely due to an augmented proliferation of VAT-Tregs, likely driven by increased TCR activation,

rather than reflecting an enhanced survival of these cells. The precise reason for this elevated TCR activation is currently unknown, but we suspect that it is related to increased maturation of, antigen-presentation by, and/or co-stimulation by antigen-presenting cells in VAT upon HFD challenge, as has been described for conventional DCs and MHCII⁺ MFs (Morris et al., 2013; Macdougall et al., 2018). This initial response of VAT-Tregs to nutritional perturbations could be a mechanism to dampen the progression of inflammation and thus safeguard organismal metabolism.

Long-term HFD feeding (>8 weeks) led to a strong reduction in VAT, but not spleen, of Treg expression of *Pparg* transcripts—both the fraction of cells expressing this nuclear receptor and the intensity of their expression. PPAR γ is known to be a major and specific orchestrator of the accumulation and phenotype of VAT-Tregs under lean conditions (Cipolletta et al., 2012). With NCD, mice lacking PPAR γ specifically in Tregs had a greatly reduced VAT (but not spleen) Treg compartment and, perhaps most relevant here, acute administration of a PPAR γ antagonist provoked rapid death of bona fide VAT (but not spleen) Tregs. Hence, the reduction of PPAR γ expression by VAT-Tregs with prolonged HFD feeding is almost certainly an important contributor to their dysregulation.

Our data also established that *IFN- α* was a key, direct driver of VAT-Treg loss during the progression of obesity. Increased production of IL-21, *IFN- γ* , or *TNF- α* , and elevated activity of STAT3, in VAT have all been suggested to underlie the dysregulation of local Tregs during obesity (Deng et al., 2017; Fabrizi et al., 2014; Priceman et al., 2013; Cipolletta et al., 2015). Ablation of whole-mouse IL-21 or T-cell-specific loss of STAT3 rescued the VAT-Treg population and improved insulin sensitivity. However, a caveat of these findings is that these mice resisted HFD-induced weight gain, so the restoration of VAT-Tregs could be secondary to differences in body and VAT weight, rather than from direct effects of these molecules on VAT-Tregs, themselves. Similarly, although implicated in the *in vivo* dysregulation of VAT-Tregs, *IFN- γ* and *TNF- α* did not directly influence VAT-Tregs in our *in vitro* culture system, arguing that these two cytokines might inhibit VAT-Treg accumulation *in vivo* through indirect mechanisms, such as through ILC2s.

In contrast, treatment of purified VAT-Tregs with *IFN- α* directly inhibited their proliferation and induced cell death, while mAb blockade of IFNAR1 signaling or Treg-specific ablation of IFNAR1 by genetic means substantially restored the accumulation of VAT-Tregs subsequent to prolonged HFD feeding and improved insulin sensitivity without affecting body weight. Previous studies investigating the influence of type-I IFNs on Tregs were mostly limited to those from lymphoid organs and the effects could be either positive or negative, depending on the context (Srivastava et al., 2014; Gangaplara et al., 2018; Kawano et al., 2018; Lee et al., 2012; Metidji et al., 2015). VAT Tregs reside in a unique tissue microenvironment and have distinct dependencies on cytokines and growth factors. Therefore, it is important to determine how type-I IFNs affect VAT Tregs

(H) Body weight (n = 6, biological replicates).

(I) ITT. Normalized blood glucose over time (left); area over the curve (AOC) (right). (n = 6, biological replicates).

Summary plots show data pooled from two to three independent experiments. Mean \pm SD.

*p < 0.05, **p < 0.01, ***p < 0.001, ****p < 0.0001 by unpaired Student's t test (A, C, D, F, I right) or two-way ANOVA (E, G, and I left).

specifically and how any effects relate to the dysregulation of VAT Tregs during obesity. Indeed, we found that the PPAR γ ⁺ subset of Tregs was especially sensitive to IFN- α -mediated inhibition, which rendered PPAR γ ⁺ VAT-Tregs particularly vulnerable to HFD challenge. Our findings are somewhat similar to a report from Hannibal et al. (Hannibal et al., 2017) that deficiencies in type-1 IFN and pDCs prevent diet-induced obesity and accompanying insulin resistance, but they differ in several important regards. For example, Hannibal et al. studied mice with a life-long, systemic loss of IFNAR1, which likely explains their observation of resistance to weight gain in the mutant mice, an unfortunate confounder. Also, they looked at effects only on myeloid cell populations.

As major producers of type-I interferons, pDCs are critical for mounting proper anti-viral immune responses but are also implicated in exacerbating certain autoimmune diseases, like systemic lupus erythematosus (Reizis et al., 2011). pDCs sense single-stranded RNA and microbial DNA via endosomal Toll-like receptor (TLR)-7 and -9, activating a MyD88-dependent signaling cascade that culminates in production of inflammatory mediators, in particular type-1 IFNs. We found that pDCs began to increase in VAT after 4 weeks of HFD feeding, which marked the onset of a regression of VAT mass, reduction in the local Treg compartment, and loss of the bona fide VAT-Treg transcriptome. Depletion of pDCs substantially restored VAT-Treg accumulation, increased their PPAR γ and ST2 expression, and improved insulin sensitivity in mice fed long-term on HFD. Thus, although VAT-Tregs initially expanded and matured to counteract HFD-induced inflammation, the progression of obesity resulted in release of extracellular DNA from dying or dead adipocytes, which was sensed by pDCs and induced them to produce large amounts of type-I IFNs, which were toxic to VAT-Tregs.

Targeting pDCs or the type-I IFN pathway might thus be a promising add-on for Treg-based therapy in the treatment of insulin resistance and metabolic diseases. This approach would allow transfer or induction of VAT-Tregs to overcome a toxic environment and to effectively exert their beneficial effects. Translation of this strategy to patients is argued by published reports of an enriched population of Tregs in human VAT and its reduction with obesity (Wu et al., 2019), of augmented levels of pDCs, type-I IFNs, and IFN-response transcripts in obese humans (Stefanovic-Racic et al., 2012; Ghosh et al., 2016), and of positive correlations between IFN-response indicators in VAT and levels of inflammatory MFs as well as both local and systemic insulin resistance (Ghosh et al., 2016).

Limitations of the study

One limitation of our study is the absence of experiments to directly translate our findings to humans. Although a reduction in Tregs and an augmentation in type-I IFN-producing pDCs in VAT from individuals with obesity have been reported, further clinical studies are required to determine whether IFN- α producing pDCs indeed directly inhibit the homeostasis of VAT-Tregs and worsen metabolic indices in subjects with obesity. In addition, the detailed molecular mechanisms by which IFN- α produced by pDCs is detrimental to PPAR γ ⁺ VAT-Tregs and why these cells are particularly sensitive to IFN- α -induced toxicity are still largely unknown and requires further investigation.

STAR★METHODS

Detailed methods are provided in the online version of this paper and include the following:

- KEY RESOURCES TABLE
- RESOURCE AVAILABILITY
 - Lead contact
 - Materials availability
 - Data and code availability
- EXPERIMENTAL MODEL AND SUBJECT DETAILS
 - Mouse models
 - Retroviral transduction and cell transfer
 - Analysis of cell proliferation and death
 - *In vivo* cytokine treatment
- METHOD DETAILS
 - *In vivo* antibody treatment
 - Depletion of plasmacytoid dendritic cells
 - Metabolic studies
 - Quantification of gene expression by RT-qPCR
 - RNA-seq library preparation and data analysis
- QUANTIFICATION AND STATISTICAL ANALYSIS

SUPPLEMENTAL INFORMATION

Supplemental information can be found online at <https://doi.org/10.1016/j.cmet.2021.06.007>.

ACKNOWLEDGMENTS

We thank A. Ortiz-Lopez, K. Hattori, L. Yang, K. Seddu, A. Mann, G. Spallanzani, T. Xiao, A. Munoz-Rojas, K. Langston, C. Laplace, C. Elkins, B. Arbaso, L. Cervantes, C. Arane, and A. Wood for experimental help and Drs. V. Kuchroo, M. Colonna, S. Gilfillan, and A. Rudensky for mouse lines. Derivation of certain mouse lines was done by the Emory Mouse Transgenic and Gene Targeting Core (supported by NIH award no. UL1TR000454). Cell sorting and flow cytometry were performed at the HSCI/DRC Flow Core (supported by NIH grant no. P30 DK036836) and Emory Flow cytometry Core (subsidized by the Emory University School of Medicine and supported by NIH award no. UL1TR002378). This work was supported by grants from the NIH (2R01 DK092541, 5RC2DK116691) and the JPB Foundation to D.M., and the Emory University School of Medicine Startup Fund to C.L.

AUTHOR CONTRIBUTIONS

Conceptualization, C.L. and D.M.; experimentation and analysis, C.L., G.W., P.S., R.N.R., and Y.Z.; original draft, C.L. and D.M.; review & editing, all authors; supervision, C.L., C.B., and D.M.; funding acquisition, C.L. and D.M.

DECLARATION OF INTERESTS

The authors declare no competing interests.

Received: April 10, 2020
 Revised: April 16, 2021
 Accepted: June 14, 2021
 Published: July 12, 2021

REFERENCES

Barrat, F.J., Crow, M.K., and Ivashkiv, L.B. (2019). Interferon target-gene expression and epigenomic signatures in health and disease. *Nat. Immunol.* 20, 1574–1583.

- Barter, R.L., and Yu, B. (2018). Superheat: an R package for creating beautiful and extendable heatmaps for visualizing complex data. *J. Comput. Graph. Stat.* *27*, 910–922.
- Bettelli, E., Carrier, Y., Gao, W., Korn, T., Strom, T.B., Oukka, M., Weiner, H.L., and Kuchroo, V.K. (2006). Reciprocal developmental pathways for the generation of pathogenic effector TH17 and regulatory T cells. *Nature* *441*, 235–238.
- Blasius, A.L., Giuriso, E., Cella, M., Schreiber, R.D., Shaw, A.S., and Colonna, M. (2006). Bone marrow stromal cell antigen 2 is a specific marker of type I IFN-producing cells in the naive mouse, but a promiscuous cell surface antigen following IFN stimulation. *J. Immunol.* *177*, 3260–3265.
- Cipolletta, D., Cohen, P., Spiegelman, B.M., Benoist, C., and Mathis, D. (2015). Appearance and disappearance of the mRNA signature characteristic of Treg cells in visceral adipose tissue: age, diet, and PPAR γ effects. *Proc. Natl. Acad. Sci. USA* *112*, 482–487.
- Cipolletta, D., Feuerer, M., Li, A., Kamei, N., Lee, J., Shoelson, S.E., Benoist, C., and Mathis, D. (2012). PPAR- γ is a major driver of the accumulation and phenotype of adipose tissue Treg cells. *Nature* *486*, 549–553.
- Deiuliis, J., Shah, Z., Shah, N., Needleman, B., Mikami, D., Narula, V., Perry, K., Hazey, J., Kampfrath, T., Kollengode, M., et al. (2011). Visceral adipose inflammation in obesity is associated with critical alterations in T regulatory cell numbers. *PLoS One* *6*, e16376.
- Deng, T., Liu, J., Deng, Y., Minze, L., Xiao, X., Wright, V., Yu, R., Li, X.C., Blaszcak, A., Bergin, S., et al. (2017). Adipocyte adaptive immunity mediates diet-induced adipose inflammation and insulin resistance by decreasing adipose Treg cells. *Nat. Commun.* *8*, 15725.
- Duerr, C.U., McCarthy, C.D., Mindt, B.C., Rubio, M., Meli, A.P., Pothlichet, J., Eva, M.M., Gauchat, J.F., Qureshi, S.T., Mazer, B.D., et al. (2016). Type I interferon restricts type 2 immunopathology through the regulation of group 2 innate lymphoid cells. *Nat. Immunol.* *17*, 65–75.
- Eller, K., Kirsch, A., Wolf, A.M., Sopper, S., Tagwerker, A., Stanzl, U., Wolf, D., Patsch, W., Rosenkranz, A.R., and Eller, P. (2011). Potential role of regulatory T cells in reversing obesity-linked insulin resistance and diabetic nephropathy. *Diabetes* *60*, 2954–2962.
- Fabrizi, M., Marchetti, V., Mavilio, M., Marino, A., Casagrande, V., Cavalera, M., Moreno-Navarrete, J.M., Mezza, T., Sorice, G.P., Fiorentino, L., et al. (2014). IL-21 is a major negative regulator of IRF4-dependent lipolysis affecting Tregs in adipose tissue and systemic insulin sensitivity. *Diabetes* *63*, 2086–2096.
- Feuerer, M., Herrero, L., Cipolletta, D., Naaz, A., Wong, J., Nayer, A., Lee, J., Goldfine, A.B., Benoist, C., Shoelson, S., and Mathis, D. (2009). Lean, but not obese, fat is enriched for a unique population of regulatory T cells that affect metabolic parameters. *Nat. Med.* *15*, 930–939.
- Gangaplara, A., Martens, C., Dahlstrom, E., Metidji, A., Gokhale, A.S., Glass, D.D., Lopez-Ocasio, M., Baur, R., Kanakabandi, K., Porcella, S.F., and Shevach, E.M. (2018). Type I interferon signaling attenuates regulatory T cell function in viral infection and in the tumor microenvironment. *PLoS Pathog.* *14*, e1006985.
- Ghosh, A.R., Bhattacharya, R., Bhattacharya, S., Nargis, T., Rahaman, O., Duttagupta, P., Raychaudhuri, D., Liu, C.S., Roy, S., Ghosh, P., et al. (2016). Adipose recruitment and activation of plasmacytoid dendritic cells fuel inflammation. *Diabetes* *65*, 3440–3452.
- Hannibal, T.D., Schmidt-Christensen, A., Nilsson, J., Fransén-Pettersson, N., Hansen, L., and Holmberg, D. (2017). Deficiency in plasmacytoid dendritic cells and type I interferon signalling prevents diet-induced obesity and insulin resistance in mice. *Diabetologia* *60*, 2033–2041.
- Hotamisligil, G.S. (2017). Foundations of immunometabolism and Implications for metabolic health and disease. *Immunity* *47*, 406–420.
- Hotamisligil, G.S., Shargill, N.S., and Spiegelman, B.M. (1993). Adipose expression of tumor necrosis factor- α : direct role in obesity-linked insulin resistance. *Science* *259*, 87–91.
- Kawano, Y., Zavidij, O., Park, J., Moschetta, M., Kokubun, K., Mouhieddine, T.H., Manier, S., Mishima, Y., Murakami, N., Bustoros, M., et al. (2018). Blocking IFNAR1 inhibits multiple myeloma-driven Treg expansion and immunosuppression. *J. Clin. Invest.* *128*, 2487–2499.
- Kolodin, D., van Panhuys, N., Li, C., Magnuson, A.M., Cipolletta, D., Miller, C.M., Wagers, A., Germain, R.N., Benoist, C., and Mathis, D. (2015). Antigen- and cytokine-driven accumulation of regulatory T cells in visceral adipose tissue of lean mice. *Cell Metab.* *21*, 543–557.
- Lee, S.E., Li, X., Kim, J.C., Lee, J., González-Navajas, J.M., Hong, S.H., Park, I.K., Rhee, J.H., and Raz, E. (2012). Type I interferons maintain Foxp3 expression and T-regulatory cell functions under inflammatory conditions in mice. *Gastroenterology* *143*, 145–154.
- Lee, Y.S., Wollam, J., and Olefsky, J.M. (2018). An integrated view of immunometabolism. *Cell* *172*, 22–40.
- Li, C., Dispirito, J.R., Zemmour, D., Spallanzani, R.G., Kuswanto, W., Benoist, C., and Mathis, D. (2018). TCR transgenic mice reveal stepwise, multi-site acquisition of the distinctive fat-Treg phenotype. *Cell* *174*, 285–299.e12.
- Li, C., Spallanzani, R.G., and Mathis, D. (2020). Visceral adipose tissue Tregs and the cells that nurture them. *Immunol. Rev.* *295*, 114–125.
- Liston, A., Nutsch, K.M., Farr, A.G., Lund, J.M., Rasmussen, J.P., Koni, P.A., and Rudensky, A.Y. (2008). Differentiation of regulatory Foxp3+ T cells in the thymic cortex. *Proc. Natl. Acad. Sci. USA* *105*, 11903–11908.
- Liu, Y.J. (2005). IPC: professional type 1 interferon-producing cells and plasmacytoid dendritic cell precursors. *Annu. Rev. Immunol.* *23*, 275–306.
- MacDougall, C.E., Wood, E.G., Loschko, J., Scagliotti, V., Cassidy, F.C., Robinson, M.E., Feldhahn, N., Castellano, L., Voisin, M.B., Marelli-Berg, F., et al. (2018). Visceral adipose tissue immune homeostasis is regulated by the crosstalk between adipocytes and dendritic cell subsets. *Cell Metab.* *27*, 588–601.e4.
- Metidji, A., Rieder, S.A., Glass, D.D., Cremer, I., Punkosdy, G.A., and Shevach, E.M. (2015). IFN- α/β receptor signaling promotes regulatory T cell development and function under stress conditions. *J. Immunol.* *194*, 4265–4276.
- Molofsky, A.B., Van Gool, F., Liang, H.E., Van Dyken, S.J., Nussbaum, J.C., Lee, J., Bluestone, J.A., and Locksley, R.M. (2015). Interleukin-33 and interferon- γ counter-regulate group 2 innate lymphoid cell activation during immune perturbation. *Immunity* *43*, 161–174.
- Moro, K., Kabata, H., Tanabe, M., Koga, S., Takeno, N., Mochizuki, M., Fukunaga, K., Asano, K., Betsuyaku, T., and Koyasu, S. (2016). Interferon and IL-27 antagonize the function of group 2 innate lymphoid cells and type 2 innate immune responses. *Nat. Immunol.* *17*, 76–86.
- Morris, D.L., Cho, K.W., Delproposto, J.L., Oatmen, K.E., Geletka, L.M., Martinez-Santibanez, G., Singer, K., and Lumeng, C.N. (2013). Adipose tissue macrophage function as antigen-presenting cells and regulate adipose tissue CD4+ T cells in mice. *Diabetes* *62*, 2762–2772.
- Nueda, M.J., Tarazona, S., and Conesa, A. (2014). Next maSigPro: updating maSigPro bioconductor package for RNA-seq time series. *Bioinformatics* *30*, 2598–2602.
- Oldenhove, G., Boucquey, E., Taquin, A., Acolty, V., Bonetti, L., Ryffel, B., Le Bert, M., Englebort, K., Boon, L., and Moser, M. (2018). PD-1 is involved in the dysregulation of type 2 innate lymphoid cells in a murine model of obesity. *Cell Rep.* *25*, 2053–2060.e4.
- Panduro, M., Benoist, C., and Mathis, D. (2016). Tissue Tregs. *Annu. Rev. Immunol.* *34*, 609–633.
- Picelli, S., Faridani, O.R., Björklund, A.K., Winberg, G., Sagasser, S., and Sandberg, R. (2014). Full-length RNA-seq from single cells using Smart-seq2. *Nat. Protoc.* *9*, 171–181.
- Platt, R.J., Chen, S., Zhou, Y., Yim, M.J., Swiech, L., Kempton, H.R., Dahlman, J.E., Parnas, O., Eisenhaure, T.M., Jovanovic, M., et al. (2014). CRISPR-Cas9 knockin mice for genome editing and cancer modeling. *Cell* *159*, 440–455.
- Priceman, S.J., Kujawski, M., Shen, S., Cherryholmes, G.A., Lee, H., Zhang, C., Kruper, L., Mortimer, J., Jove, R., Riggs, A.D., et al. (2013). Regulation of adipose tissue T cell subsets by Stat3 is crucial for diet-induced obesity and insulin resistance. *Proc. Natl. Acad. Sci. USA* *110*, 13079–13084.
- Prigge, J.R., Hoyt, T.R., Dobrinen, E., Capecci, M.R., Schmidt, E.E., and Meissner, N. (2015). Type I IFNs act upon hematopoietic progenitors to protect and maintain hematopoiesis during pneumocystis lung infection in mice. *J. Immunol.* *195*, 5347–5357.

- Reizis, B., Bunin, A., Ghosh, H.S., Lewis, K.L., and Sisirak, V. (2011). Plasmacytoid dendritic cells: recent progress and open questions. *Annu. Rev. Immunol.* *29*, 163–183.
- Rosen, E.D., and Spiegelman, B.M. (2014). What we talk about when we talk about fat. *Cell* *156*, 20–44.
- Rubtsov, Y.P., Rasmussen, J.P., Chi, E.Y., Fontenot, J., Castelli, L., Ye, X., Treuting, P., Siewe, L., Roers, A., Henderson, W.R., Jr., et al. (2008). Regulatory T cell-derived interleukin-10 limits inflammation at environmental interfaces. *Immunity* *28*, 546–558.
- Spallanzani, R.G., Zemmour, D., Xiao, T., Jayewickreme, T., Li, C., Bryce, P.J., Benoist, C., and Mathis, D. (2019). Distinct immunocyte-promoting and adipocyte-generating stromal components coordinate adipose tissue immune and metabolic tenors. *Sci. Immunol.* *4*, eaaw3658.
- Srivastava, S., Koch, M.A., Pepper, M., and Campbell, D.J. (2014). Type I interferons directly inhibit regulatory T cells to allow optimal antiviral T cell responses during acute LCMV infection. *J. Exp. Med.* *211*, 961–974.
- Stefanovic-Racic, M., Yang, X., Turner, M.S., Mantell, B.S., Stolz, D.B., Sumpter, T.L., Sipula, I.J., Dedousis, N., Scott, D.K., Morel, P.A., et al. (2012). Dendritic cells promote macrophage infiltration and comprise a substantial proportion of obesity-associated increases in CD11c+ cells in adipose tissue and liver. *Diabetes* *61*, 2330–2339.
- Subramanian, A., Tamayo, P., Mootha, V.K., Mukherjee, S., Ebert, B.L., Gillette, M.A., Paulovich, A., Pomeroy, S.L., Golub, T.R., Lander, E.S., and Mesirov, J.P. (2005). Gene set enrichment analysis: a knowledge-based approach for interpreting genome-wide expression profiles. *Proc. Natl. Acad. Sci. USA* *102*, 15545–15550.
- Swiecki, M., Gilfillan, S., Vermi, W., Wang, Y., and Colonna, M. (2010). Plasmacytoid dendritic cell ablation impacts early interferon responses and antiviral NK and CD8+ T cell accrual. *Immunity* *33*, 955–966.
- Trapnell, C., Roberts, A., Goff, L., Pertea, G., Kim, D., Kelley, D.R., Pimentel, H., Salzberg, S.L., Rinn, J.L., and Pachter, L. (2012). Differential gene and transcript expression analysis of RNA-seq experiments with TopHat and Cufflinks. *Nat. Protoc.* *7*, 562–578.
- Vasanthakumar, A., Moro, K., Xin, A., Liao, Y., Gloury, R., Kawamoto, S., Fagarasan, S., Mielke, L.A., Afshar-Sterle, S., Masters, S.L., et al. (2015). The transcriptional regulators IRF4, BATF and IL-33 orchestrate development and maintenance of adipose tissue-resident regulatory T cells. *Nat. Immunol.* *16*, 276–285.
- Wu, D., Han, J.M., Yu, X., Lam, A.J., Hoeppli, R.E., Pesenacker, A.M., Huang, Q., Chen, V., Speake, C., Yorke, E., et al. (2019). Characterization of regulatory T cells in obese omental adipose tissue in humans. *Eur. J. Immunol.* *49*, 336–347.

STAR★METHODS

KEY RESOURCES TABLE

REAGENT or RESOURCE	SOURCE	IDENTIFIER
Antibodies		
anti-CD45.1 (clone A20)	Biolegend	Cat# 110724; RRID: AB_493733
anti-CD45.2 (clone 104)	Biolegend	Cat# 109824; RRID: AB_830789
anti-CD3 (clone 17A2)	Biolegend	Cat# 100214; RRID: AB_493645
anti-CD4 (clone GK1.5)	Biolegend	Cat# 100422; RRID: AB_312707
anti-CD25 (clone PC61)	Biolegend	Cat# 102026; RRID: AB_830745
anti-KLRG1 (clone 2F1/KLRG1)	Biolegend	Cat# 138416; RRID: AB_2561736
anti-IFNAR1 (clone MAR1-5A3)	Biolegend	Cat# 127312; RRID: AB_2248800
anti-TCR V α 2 (clone B20.1)	Biolegend	Cat# 127806; RRID: AB_1134188
anti-CD45 (clone 30-F11)	Biolegend	Cat# 103126; RRID: AB_493535
anti-CD11b (clone M1/70)	Biolegend	Cat# 101230; RRID: AB_2129374
anti-CD11c (clone N418)	Biolegend	Cat# 117310; RRID: AB_313779
anti-F4/80 (clone BM8)	Biolegend	Cat# 123114; RRID: AB_893478
anti-CD19 (clone 1D3/CD19)	Biolegend	Cat# 152408; RRID: AB_2629817
anti-PDCA1 (clone 927)	Biolegend	Cat# 127014; RRID: AB_1953289
anti-B220 (clone RA3-6B2)	Biolegend	Cat# 103232; RRID: AB_493717
anti-SiglecH (clone 551)	Biolegend	Cat# 129606; RRID: AB_2189147
anti-Ly6c (clone HK1.4)	Biolegend	Cat# 128005; RRID: AB_1186134
anti-ST2 (clone RMST2-2)	eBioscience	Cat# 46-9335-80; RRID: AB_2573882
anti-Foxp3 (clone FJK-16s)	eBioscience	Cat# 17-5773-82; RRID: AB_469457
anti-TCR V β 4 (clone KT4)	BD Biosciences	Cat# 553366; RRID: AB_394812
anti-Thy1.1 (clone OX-7)	BD Biosciences	Cat# 561409; RRID: AB_10683163
anti-Thy1.2 (clone 53-2.1)	BD Biosciences	Cat#561641; RRID: AB_10898013
<i>InVivo</i> MAB anti-IFNAR1 (clone MAR1-5A3)	BioXCell	Cat# BE0241; RRID: AB_2687723
<i>InVivo</i> MAB IgG1 isotype control (clone MOPC-21)	BioXCell	Cat# BE0083; RRID: AB_1107784
<i>InVivo</i> MAB anti-PDCA1 (clone 927)	BioXCell	Cat# BE0311; RRID: AB_2736991
<i>InVivo</i> MAB IgG2b isotype control (clone LTF-2)	BioXCell	Cat# BE0090; RRID: AB_1107780
Chemicals, peptides, and recombinant proteins		
Recombinant Human IL-2	Peptotech	Cat# 200-02
Recombinant mouse IL-33 (carrier-free)	Biolegend	Cat# 580506
Recombinant Mouse IFN- α (carrier-free)	Biolegend	Cat# 752806
Recombinant Mouse TNF- α (carrier-free)	Biolegend	Cat# 575206
Recombinant Mouse IFN- γ (carrier-free)	Biolegend	Cat# 575306
Insulin	Eli Lilly	Humulin R U-100
D-Glucose	Thermo Fisher	Cat# D16-500
Collagenase type II	Sigma	Cat# C6885
2-Mercaptoethanol	Sigma	Cat# M7522
Diphtheria Toxin	Sigma	Cat# D0564
Critical commercial assays		
Foxp3 / Transcription Factor Staining Buffer Set	eBioscience	Cat# 00-5523-00
TransIT-293 Transfection Reagent	Mirus	Cat# MIR 2705
Click-iT Plus EdU Pacific Blue Flow Cytometry Assay Kit	Invitrogen	Cat# C10636

(Continued on next page)

Continued		
REAGENT or RESOURCE	SOURCE	IDENTIFIER
LIVE/DEAD Fixable Near-IR Dead Cell Stain Kit	Invitrogen	Cat# L10119
Annexin V	Biolegend	Cat# 640920
Annexin V Binding Buffer	Biolegend	Cat# 422201
SuperScript III Reverse Transcriptase	Invitrogen	Cat# 18080093
Dynabeads Untouched Mouse CD4 Cells Kit	Thermo Fisher	Cat# 11415D
Dynabeads Mouse T-Activator CD3/CD28 for T-Cell Expansion and Activation	Thermo Fisher	Cat# 11453D
RNeasy Lipid Tissue Mini Kit	Qiagen	Cat# 74804
RNAClean XP beads	Beckman Coulter	Cat# A63987
Nextera DNA Sample Prep Kit	Illumina	Cat# FC-121-1030
Deposited data		
RNA-Seq data	This paper	GSE174706
Experimental models: Cell lines		
Platinum-E Retroviral Packaging Cell Line	CELL BIOLABS	RV-101
Experimental models: Organisms/strains		
Mouse: vTreg53 TCR Tg / B6	Li et al., 2018	N/A
Mouse: Pparg-Tdt / B6	Li et al., 2018	N/A
Mouse: B6.CD45.1	Jackson Laboratory	002014
Mouse: B6.CD45.2	Jackson Laboratory	000664
B6.Foxp3-cre	Jackson Laboratory	016959
B6.Rosa26-Cas9	Jackson Laboratory	026179
B6.Ifnar1fl	Jackson Laboratory	028256
Mouse: B6. Foxp3-GFP	Bettelli et al., 2006	N/A
Mouse: B6. Foxp3-Thy1.1	Liston et al., 2008	N/A
Mouse: B6.Bdca2-Dtr	Swiecki et al., 2010	N/A
Oligonucleotides		
sgRNA targeting <i>Ifnar1</i> sequence: 5' CTTCTAAACGTACTTCTGGG 3'	This paper	N/A
qPCR primer for Tbp FWD: 5' ACCCTTACCAATGACTCCTATG	This paper	N/A
qPCR primer for Tbp REV: 5' TGACTGCAGCAAATCGCTTGG	This paper	N/A
qPCR primer for <i>Itna</i> FWD: 5' CCTGCTGGCTGTGAGGA	This paper	N/A
qPCR primer for <i>Itna</i> REV: 5' GGAAGACAGGGCTCTCCAG	This paper	N/A
Recombinant DNA		
Plasmid: MSCV-Ctl-sg-GFP	This paper	N/A
Plasmid: MSCV-Ctl-sg-RFP	This paper	N/A
Plasmid: MSCV-Ifnar1-sg-GFP	This paper	N/A
Software and algorithms		
Cuffquant version 2.2.1	Trapnell et al., 2012;	http://cole-trapnell-lab.github.io/cufflinks/install/
GenePattern software package	Broad Institute	http://software.broadinstitute.org/cancer/software/genepattern/
R	The R Foundation	https://www.r-project.org
GSEA	Broad Institute	http://www.gsea-msigdb.org/gsea/index.jsp

(Continued on next page)

Continued

REAGENT or RESOURCE	SOURCE	IDENTIFIER
PRISM	GraphPad	https://www.graphpad.com
FlowJo	FlowJo	https://www.flowjo.com
Other		
NCD: Picolab Mouse Diet 20 with 13 kcal % Fat	Lab Diet	No. 5053
HFD: Rodent Diet With 60 kcal% Fat	Research Diets	Cat#: D12492

RESOURCE AVAILABILITY**Lead contact**

Further information and requests for resources and reagents should be directed to and will be fulfilled by the lead contact, Diane Mathis (Diane_Mathis@hms.harvard.edu).

Materials availability

All unique/stable reagents generated in this study are available from the lead contact with a completed Materials Transfer Agreement.

Data and code availability

The accession number for the RNA sequencing data reported in this paper is GEO: GSE174706.

EXPERIMENTAL MODEL AND SUBJECT DETAILS**Mouse models**

Male mice were produced in our specific-pathogen-free facilities at Harvard Medical School or Emory University School of Medicine and were fed an NCD (13 kcal% fat, no. 5053, Lab Diet Picolab Mouse Diet 20) until 10-12 weeks of age. They were then either continued on an NCD or switched to an HFD (60 kcal% fat, D12492, Research Diets) for 2, 4, 8, or 16 weeks. Mice were housed in a temperature (22-24°C)-controlled colony room with a 12-h light/dark cycle under specific-pathogen-free (SPF) conditions. Littermates were used for all experiments. B6.CD45.2⁺ (000664), B6.CD45.1⁺ (002014), B6.Rosa26-Cas9 (026179) (Platt et al., 2014), B6.*Ifnar1*^{fl} (028256) (Prigge et al., 2015) and B6.*Foxp3-cre* (016959) (Rubtsov et al., 2008) mice were obtained from the Jackson Laboratory. vTreg53 TCR-tg and *Pparg-tdT* mice were generated on the B6 background in our laboratory as previously described (Li et al., 2018). *Foxp3-GFP* (Bettelli et al., 2006) and *Foxp3-Thy1.1* (Liston et al., 2008) mice were obtained from Dr. A. Rudensky and were maintained on the B6 background. B6.*Bdca2-Dtr* mice were obtained from Dr. M. Colonna and rederived by the Mouse Transgenic and Gene Targeting Core at Emory University. All experiments were performed using littermate controls and repeated at least twice. The animal protocols were approved by the HMS Institutional Animal Use and Care Committee (IACUC) (protocol IS00001257) and Emory University IACUC (PROTO201900197).

Retroviral transduction and cell transfer

Treg cells were sorted from pooled spleen and lymph nodes of 6-8-week-old male CD45.1⁺CD45.2⁺ TCR-tg *Cas9*^{KI/WT} *Foxp3-thy1.1*^{KI/y} mice, stimulated with Dynabeads™ Mouse T-Activator CD3/CD28 for T-Cell Expansion and Activation (Invitrogen) at 37°C in a 5% CO₂ humid atmosphere, transduced with retrovirus expressing sgRNA targeting *Ifnar1* or a control non-targeting sgRNA, and were intravenously (*i.v.*) transferred (0.2x10⁶ per mouse) into 12-week-old male CD45.1⁺CD45.2⁺ *Cas9*^{KI/WT} recipients previously fed with NCD. In one set of experiment, both the *Ifnar1*- and *Ctl*-sgRNA expressing constructs also encoded GFP, and transduced cells were transferred into separate groups of recipient mice subsequently fed with either NCD or HFD for 8 weeks. In another set of experiments, the *Ifnar1*-sgRNA construct co-expressed GFP, while the *Ctl*-sgRNA construct co-expressed mRFP. The transduced cells were mixed at a 1:1 ratio, and the mixture was transferred into recipient mice subsequently fed on HFD for 8 weeks.

Analysis of cell proliferation and death

For monitoring of cell division *in vivo*, 40 µg/g body weight EdU (Invitrogen) was intraperitoneally (*i.p.*) injected into mice fed with NCD or HFD, and 5 hrs later, cells were processed for detection by the Click-iT Plus EdU Cell Proliferation Kit following the manufacturer's instructions (Invitrogen). For detection of Treg-cell death directly *ex vivo*, freshly isolated cells were stained with fluorochoime-labeled Annexin V according to the manufacturer's instructions (BioLegend). For monitoring of VAT-Treg cell division *in vitro*, PPARγ⁺ Treg cells were sorted from VAT of 8-10-week-old *Pparg-tdT*^{KI/KI} *Foxp3-GFP*^{KI/y} male mice that were injected with 2ug recombinant mouse IL-33 (BioLegend) twice in a week, and were cultured in the presence of 2000 U/ml recombinant human IL-2 (Peprotech) and 10 ng/ml IL-33 with or without 50ng/ml TNFα, IFNγ, or IFNα (BioLegend) for 4 days at 37°C in a 5% CO₂ humid atmosphere.

In the last 2 hrs of culture, cells were pulsed with 10 μ M EdU, and cell proliferation and death were detected by the Click-iT Plus EdU Cell Proliferation Kit and LIVE/DEAD Fixable Near-IR Dead Cell Stain Kit, respectively.

In vivo cytokine treatment

For *in vivo* cytokine treatment, 8-week-old B6 or *Pparg*-*tdT* *Foxp3*-GFP male mice were *i.p.*-injected with 2 μ g TNF α , IFN γ , or IFN α with or without 2 μ g IL-33 twice in a week. The frequencies and numbers of spleen- and VAT-Treg cells as well as ILC2s were analyzed on day 7 after the first injection.

METHOD DETAILS

Male mice were asphyxiated with CO₂ and perfused with 10-20ml of phosphate-buffered saline (PBS). Epididymal VAT was excised, minced, and digested for 20 min with 1.5 mg/ml collagenase type II (Sigma) in Dulbecco's Modified Eagle's Medium (DMEM) supplemented with 2% fetal calf serum (FCS) in a 37°C water bath with shaking. The digested materials were filtered through a sieve and then a 40 μ m nylon cell strainer, and the stromal vascular fraction (SVF) was collected after centrifugation at 450 x g for 10 min. For T lymphocyte analysis, cells were stained with anti-CD45.1 (A20), -CD45.2 (104), -CD3 (17A2), -CD4 (GK1.5), -CD25 (PC61), -KLRG1 (2F1/KLRG1), -IFNAR1 (MAR1-5A3), and/or -TCR V α 2 (B20.1) mAbs (all from BioLegend); anti-ST2 (RMST2-2) (eBioscience); anti-TCR V β 4 (KT4), -Thy1.1 (OX-7), and/or -Thy1.2 (53-2.1) mAbs (all from BD Biosciences), and/or LIVE/DEAD Fixable Violet Dead Cell Stain Kit (Invitrogen). Cells were either fixed, permeabilized, and intracellularly stained for *Foxp3* (FJK-16 s) according to the manufacturer's instructions (eBioscience) or were fixed by 2% paraformaldehyde (PFA) in PBS for 20 min before analysis. For myeloid cell analysis, cells were stained with anti-CD45 (30-F11), -CD11b (M1/70), -CD11c (N418), -F4/80 (BM8), -CD19 (1D3/CD19), -PDCA1 (927), -B220 (RA3-6B2), -SiglecH (551), and/or -Ly6c (HK1.4) mAbs (all from BioLegend). All Abs were used at a 1 to 100 dilution for staining. Cells were acquired with LSRII or FACSymphony A3 flow cytometers (BD Biosciences) and sorted with MoFlo Astrios EQ cell sorter or MoFlo Legacy (Beckman Coulter), Data were analyzed using FlowJo software.

In vivo antibody treatment

For the IFNAR1-blockade experiments, 12-week-old male vTreg53 TCR-tg mice were fed with HFD, and were injected *i.p.* with 250 μ g anti-mouse IFNAR1 mAb (BioXCell, clone MAR1-5A3) or mouse IgG1 isotype control (BioXCell, clone MOPC-21) twice a week for 8 weeks. Any effects of the Ab treatments on metabolic parameters were determined 7 weeks after the introduction of HFD, and the mice were euthanized for flow cytometric analysis 8 weeks after HFD introduction.

Depletion of plasmacytoid dendritic cells

For the pDC-depletion experiments using anti-PDCA-1 Ab, 12-week-old male vTreg53 TCR-tg mice were fed with HFD, and were injected *i.p.* with 250ug anti-mouse PDCA-1 (BioXcell, clone 927) or Rat IgG2b isotype control (BioXCell, clone LTF-2) twice a week for 8 weeks. For the pDC-depletion experiments using *Bdca2-Dtr* mice, 10-week-old *Bdca2-Dtr*⁺ or *Dtr*⁻ male mice were fed on HFD for 4 weeks and were then continued on HFD and injected *i.p.* with 5ng/g body weight DT (Sigma) twice a week for another 4 weeks. Any effects of pDC depletion on metabolic parameters were determined 7 weeks after the introduction of HFD, and the mice were euthanized for flow cytometric analysis 8 weeks after HFD introduction.

Metabolic studies

10-12-week-old male mice with specific genotypes were fed with HFD, and were injected *i.p.* with mAbs twice a week for 8 weeks, or injected *i.p.* with DT twice a week for 4 weeks (between 5 and 8 weeks after HFD treatment). At 7 weeks after the introduction of HFD, mice were subjected to an insulin tolerance test (ITT). Briefly, they were fasted for 4 hours before being injected *i.p.* with insulin (1 unit/kg body weight, Humulin R, Lilly). Blood-glucose levels were measured before and 20, 40, 60, 90, and 120 minutes after insulin injection, and were normalized to the blood-glucose levels before insulin injection. Area over the curve (AOC) was calculated using GraphPad Prism.

Quantification of gene expression by RT-qPCR

RNA from adipose tissue was extracted and purified using RNeasy Lipid Tissue Mini Kit (QIAGEN) according to the manufacturer's instructions. cDNA was synthesized using SuperScript II Reverse Transcriptase (Thermo Fischer Scientific). Real-time quantitative PCR was performed using SYBR Green-based assays (Applied Biosystems). Transcript values were normalized to those from the mouse *Tbp* gene (FWD: ACCCTTCACCAATGACTCCTATG; REV: TGA CTGCAGCAAATCGCTTGG). A primer set that detects most *Ifna* isoforms was employed for PCR titration of transcript levels (FWD: CCTGCTGGCTGTGAGGA; REV: GGAAGACAGG GCTCTCCAG).

RNA-seq library preparation and data analysis

For the HFD time-course experiment, 12-week-old male vTreg53 TCR-tg *Foxp3*-GFP^{KI/y} mice were fed with either NCD or HFD for 2, 4, 8, or 16 weeks, and biological replicates of 1,000 clonotype⁺ spleen- or VAT-Treg cells were double-sorted by Moflo into 5ul Buffer TCL (QIAGEN) with 1% 2-Mercaptoethanol (Sigma). For the IFN α treatment experiments, PPAR γ ⁺ Treg cells were sorted from VAT of 8-10-week-old *Pparg*-*tdT*^{KI/KI} *Foxp3*-GFP^{KI/y} male mice injected with 2 μ g IL-33 twice in a week, and were cultured in the presence of

2000 U/ml IL-2 and 10 ng/ml IL-33 with or without 50ng/ml IFN α . Three days after culture, biological replicates of 1,000 Treg cells were double-sorted by Moflo into 5ul Buffer TCL (QIAGEN) with 1% 2-Mercaptoethanol (Sigma). Smart-Seq2 libraries were prepared by the Broad Technology Labs, and were sequenced using the Broad Genomics Platform (Picelli et al., 2014). Briefly, total RNA was captured and purified on RNAClean XP beads (Beckman Coulter). Polyadenylated mRNA was then selected using an anchored oligo(dT) primer and converted to cDNA via reverse transcription. First-strand cDNA was subjected to limited PCR amplification, followed by transposon-based fragmentation using the Nextera XT DNA Library Preparation Kit (Illumina). Samples were then PCR-amplified using bar-coded primers such that each sample carried a specific combination of Illumina P5 and P7 bar-codes and were pooled prior to sequencing. Sequencing was performed on an Illumina NextSeq500 instrument using 2x25bp or 2x38bp reads. Transcripts were quantified by the Broad Technology Labs computational pipeline with Cuffquant version 2.2.1 (Trapnell et al., 2012). Normalized reads were further filtered by minimal expression and coefficient of variation. Data were analyzed by Population PCA and Multiplot Studio in the GenePattern software package and GSEA (Subramanian et al., 2005). To identify gene expression dynamics across HFD and NCD time-series data, a two-step regression modeling strategy using maSigPro was applied (Nueda et al., 2014). An alpha of 0.05 was selected to account for multiple hypothesis testing and a false discovery rate of 5% were applied to first identify differential gene expression. To identify co-expression of genes during the time-series, silhouette analysis partitioned significant genes into 5 clusters (cluster correlation, $r^2 > 0.65$), and visualized as heatmaps (Barter and Yu, 2018). Compilation of the VAT-Treg signature gene-sets was described previously (Cipolletta et al., 2015).

QUANTIFICATION AND STATISTICAL ANALYSIS

Data were routinely presented as mean \pm SD. Normal distribution of populations at the 0.05 level was calculated. Unless stated otherwise, significance was assessed by Student's t-test for two-groups comparisons or ANOVA for multiple-group comparisons using GraphPad Prism 7.0. To determine the enrichment of certain gene signatures in RNA-seq data-sets, we used a Chi-square test. $P = *$, < 0.05 ; $**$, < 0.01 ; $***$, < 0.001 ; $****$, < 0.0001 . n represents the number of mice and is reported in the figure legends. Mice with the same genotypes were assigned randomly to groups. No samples were excluded and blinding methods were not used. No statistical method was used to predetermine sample size. Sample sizes were chosen based on similar previous publications (Kolodin et al., 2015). Data showed a continuous normal distribution.